remote sensing

MDPI

Article

Comparison of Terrestrial Water Storage Changes in the Tibetan Plateau and Its Surroundings Derived from Gravity Recovery and Climate Experiment (GRACE) Solutions of Different Processing Centers

Longwei Xiang [1,2,*], Holger Steffen [3] and Hansheng Wang [2]

[1] School of Geosciences, Yangtze University, Wuhan 430100, China
[2] State Key Laboratory of Geodesy and Earth's Dynamics, Innovation Academy for Precision Measurement Science and Technology, Chinese Academy of Sciences, Wuhan 430077, China; whs@whigg.ac.cn
[3] Geodetic Infrastructure, Lantmäteriet, 80182 Gävle, Sweden; holger.steffen@lm.se
* Correspondence: lwxiang@yangtzeu.edu.cn

Abstract: The GRACE twin satellite gravity mission from 2002 to 2017 has considerably improved investigations on global and regional hydrological changes. However, there are different GRACE solutions and products available which may yield different results for certain regions despite applying the same postprocessing and time span. This is especially the case for the Tibetan Plateau (TP) with its special hydrological conditions represented by localized but strong signals that can overlap or merge with signals inside the plateau, which can falsify the determination of terrestrial water storage (TWS) changes in the TP area. To investigate the effect of GRACE solution selection on inverted TWS changes, we analyze quantitatively the secular and monthly changes for 14 glacier areas and 10 water basins in and around the TP area that have been calculated from 16 different available GRACE solutions. Our analysis provides expectable results. While trend results from different spherical harmonic (SH) GRACE solutions match well, there are significant differences to and between mascon GRACE solutions. This is related to the different processing concepts of mascon solutions and their forced handling in our comparisons. SH solution time series match each other when mass changes are strong with a large amplitude and regular periodicity. However, for regions where small TWS changes are associated with small amplitudes, trends, and/or unstable signal periods, SH solutions can also yield different results. Such behavior is known from a time series analysis. Interestingly though, we find that the COST-G and ITSG SH GRACE solutions are closest to the average of all solutions. Therefore, these solutions appear to be preferable for TWS investigations in regions with highly variable hydrological conditions, such as in the Tibetan Plateau and its surroundings. This also indicates that combined solutions such as COST-G provide a promising pathway for an improved TWS analysis, which should be further elaborated.

Keywords: satellite gravity; GRACE solution; Tibetan Plateau and its surroundings; terrestrial water storage change; regional hydrology

Citation: Xiang, L.; Steffen, H.; Wang, H. Comparison of Terrestrial Water Storage Changes in the Tibetan Plateau and Its Surroundings Derived from Gravity Recovery and Climate Experiment (GRACE) Solutions of Different Processing Centers. *Remote Sens.* **2023**, *15*, 5417. https://doi.org/10.3390/rs15225417

Academic Editors: Mirko Reguzzoni, Mehdi Eshagh and Carla Braitenberg

Received: 28 September 2023
Revised: 13 November 2023
Accepted: 14 November 2023
Published: 18 November 2023

1. Introduction

The Tibetan Plateau (TP) in Central Asia is a unique area. Geographically, it is both the highest and the largest plateau in the world. Hydrologically, it contains the largest ice fields outside of the Arctic and Antarctica, as well as a wide distribution of natural lakes and permafrost, so that it is often regarded as 'the water tower of Asia' [1–7]. The climatic conditions in the TP and its surroundings are governed by the Indian monsoon and the westerlies in the summer and winter, respectively, as well as the East Asian monsoon [3,8–10]. Global warming and changes in the atmospheric circulation patterns

have led to severe hydrological changes in recent decades, such as continual lake expansion [1,11], glacier (and snow) retreat [12,13], changes in soil moisture [14,15], and permafrost degradation [6], ultimately increasing groundwater [16].

The Gravity Recovery and Climate Experiment (GRACE) twin-satellite mission is a very reliable and convenient tool to determine terrestrial water storage (TWS) changes in the TP as it helps to overcome the sparsity of ground measurements. The mission was launched in 2002, and the GRACE results were originally provided by three institutions, namely the Center of Space Research (CSR) in Austin, Texas, USA, the Jet Propulsion Laboratory (JPL) in Pasadena, California, USA, and the Geoforschungszentrum (GFZ) in Potsdam, Germany, in the form of spherical harmonic (SH) coefficients that are part of the so-called Level-2 products calculated from earlier processed Level-0, Level-1A, and Level-1B products; here, basically, binary encoded satellite measurements together with other data are converted, preprocessed, and combined to correctly obtain time-tagged and sample-rate-reduced results with appropriate units. Then, adequate postprocessing must be applied to calculate gravity changes and to extract the signal of interest. Over the last two decades, more institutions have started providing Level-2 and even Level-3 products. The latter are already postprocessed gravity changes which are ready for analysis. The large amount of more than a dozen various Level-2 and -3 products may confuse a potential user because each product is based on different processing strategies with different corrections. Moreover, results may show significant discrepancies as has been found for the TP [17,18]. Measurement noises, orbit errors, and different strategies for producing GRACE solutions have led to inconsistencies among different solutions. Furthermore, the special hydrological conditions that small TWS changes are surrounded by much larger glacier melting and groundwater extraction can disturb TWS signals inside the plateau by stronger surrounding TWS signals during a data inversion.

Xiang et al. [17] tested a large set of GRACE solution-filter combinations and mascon models to identify the best combination whose filtered results matched the produced (so-called) aggregated hydrology signals (AHS) of TWS changes based on independent hydrological observations, however, the tests were limited to a trend analysis because not enough reliable observations and model data were available. In addition, the comparison results were rather preliminary compared to the TWS changes in water basins. Therefore, on the basis of the results of Xiang et al. [17], we study the effects of the selection of a GRACE solution on basin-scale inverted TWS changes in the Tibetan Plateau and its surroundings. We select 14 glacier areas and 10 water basins (see Figure 1) according to Xiang et al. [19] and provide basin-scale inverted TWS changes time series. Note that our focus is a comparison of the different products to identify those with the best performance. We are not discussing the results of TWS changes in detail, nor do we compare them with the results of previous studies. In Section 2, the GRACE solutions, destriping filters, as well as the inversion approach are briefly introduced. We present and discuss the results in Section 3. Finally, we summarize our findings in Section 4.

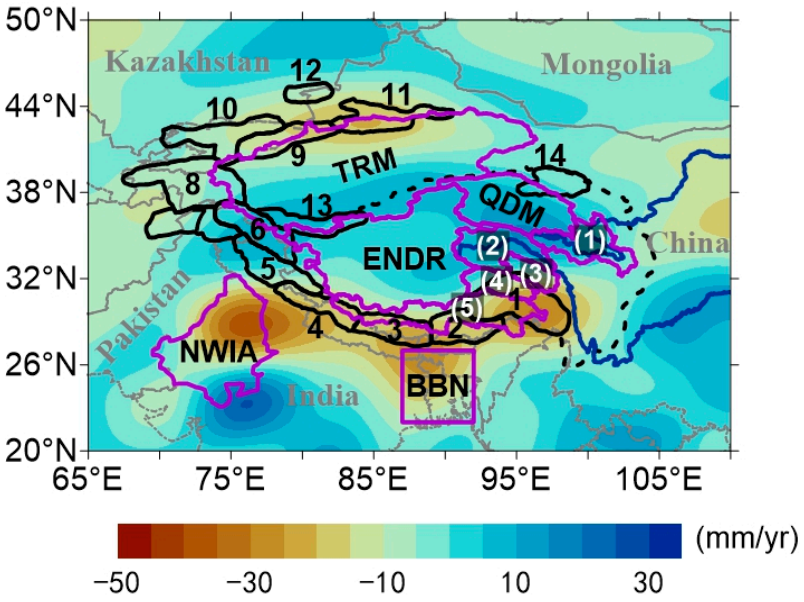

Figure 1. Distribution of 14 glacier mascons (black number 1–14) and 10 water basins (abbreviations and white numbers) in the Tibetan Plateau and its surroundings. The filled contours are the TWS change trends derived from COST-G from January 2003 to December 2015. The unit is mm/year in equivalent water column. The 14 glacier mascons (number 1–14) together with the dashed lines delimit the TP and Tien Shan. Purple lines delimit water basins. Grey lines are the national boundaries, while the blue lines indicate the Yangtze River and the Yellow River, respectively. NWIA, Northwest India; BBN, Bengal Basin; TRM, Tarim Basin; QDM, Qaidam Basin; ENDR, Endorheic Region of the TP; (1), YLRS, Yellow River source region; (2), YZRS, Yangtze River source region; (3), MKRS: Mekong River source region; (4), SWRS, Salween River source region; (5), YZBR, Yarlung Zangbo River Basin.

2. Data and Methodology

We investigate GRACE Level-2 and Level-3 products, which we introduce in the next Section 2.1. The Level-2 SH solutions need dedicated processing with destriping filters to show the spatial TWS changes. This is explained in Section 2.2. For comparison with Level-3 mascon solutions, the TWS changes from the SH solutions must be inverted to basin scale, i.e., the special mascons shown in Figure 1. Our computation approach for this inversion is presented in Section 2.3.

2.1. GRACE Solutions

From the many different GRACE products that are currently available (see e.g., http://icgem.gfz-potsdam.de/series, accessed on 17 April 2023 for the SH solutions), we selected the 12 most commonly used SH solutions (Level-2 products) and four so-called mascon solutions (Level-3 products) (Table 1). All the products have different start and end dates but cover the time span between January 2003 and December 2015, therefore, we set this as our time span.

The 12 SH solutions are provided with different maximum degree/order (d/o) Stokes coefficients and need destriping and spatial smoothing filters to reduce the high-frequency noises and correlated errors (see Section 2.2). The common spectral range is from 2 to 60, and thus was used here. The glacial isostatic adjustment (GIA) effects were removed from the monthly Stokes coefficients according to the GIA model ICE-6G_C(VM5a) [20]. Considering the absence of degree-1 coefficients (C10, C11, and S11) and inaccuracy of C20 (degree 2 order 0) and C30 (degree 3 order 0), we complemented the GRACE SH solutions with newly released C10, C11, and S11 coefficients [21], and replaced the native GRACE C20 and C30 coefficients with the latest SLR-derived version [22]. We note that the C30 coefficients were replaced when the time series passed March 2012, where the SLR-derived C30 starts in the data set according to Loomis et al. [22].

The four mascon solutions provide gridded TWS changes. As they are Level-3 products, they can be used directly without further processing but have different accuracies and spatial resolutions due to different strategies in their development. For the comparison in our study, all four mascon solution grids were regridded to match the mascons outlined in Figure 1.

Table 1. Information of the 16 different GRACE solutions used in this study. The organizations are expressed in abbreviations. The resolution is maximum degree/order Stokes coefficients of different versions for SH solutions and spatial resolutions for mascon solutions.

GRACE Solution	Organization	Time Span	Resolution	Reference
ITSG	TU Graz	April 2002–June 2017	60, 96, 120	Kvas et al. [23]
CSR	UT CSR	April 2002–June 2017	60, 96	Bettadpur et al. [24]
COST-G	AIUB	April 2002–June 2017	90	Meyer et al. [25]
GFZ	GFZ	April 2002–June 2017	60, 96	Dahle et al. [26]
JPL	JPL	April 2002–June 2017	60, 96	Watkins et al. [27]
Tongji	TJU	April 20024–August 2016	96	Chen et al. [28]
WHU	WHU	August 2002–July 2016	96	Zhong et al. [29]
HUST	HUST	January 2003–July 2016	60, 90	Zhou et al. [30]
GRGS	CNES-GRGS	September 2002–May 2017	90	Lemoine et al. [31]
IGG	IGG	April 2002–July 2016	60	Wang et al. [32]
AIUB	AIUB	April 2002–June 2017	90	Darbeheshti et al. [33]
XISM	XISM&SSTC	April 2002–March 2016	60	Xiao et al. [34]
CSR_M	UT CSR	April 2002–June 2017	1°	Save et al. [35]
JPL_M	JPL	April 2002–June 2017	3°	Watkins et al. [27]
GSFC_M	NASA/GSFC	January 2003–July 2016	1°	Loomis et al. [36]
ANU_M	ANU	August 2002–July 2016	3°, 2°	Tregoning et al. [37]

Note: Organization abbreviations are defined as follows: TU Graz, Graz University of Technology; UT CSR, Center for Space Research, University of Texas at Austin; AIUB, Astronomical Institute University of Bern; GFZ, GFZ German Research Centre for Geosciences; JPL, NASA Jet Propulsion Laboratory; TJU, Tongji University; WHU, Wuhan University; HUST, Huazhong University of Science and Technology; CNES-GRGS, Centre National d'Etudes Spatiales, Groupe de Recherches de Géodésie Spatiale; IGG, Institute of Geodesy and Geophysics, Chinese Academy of Sciences; XISM&SSTC, Xian Research Institute of Surveying and Mapping and Space Star Technology Co., LTD.; NASA/GSFC, NASA Goddard Space Flight Center; ANU, Australian National University, Canberra, ACT, Australia.

2.2. Destriping Filters

According to Xiang et al. [17], 'S&W P3M8' proposed by Swenson and Wahr [38] for destriping together with a 340 km averaging radius Gaussian smoothing filter [39] have been found to be the best filter combination for the identification of TWS changes in the Tibetan Plateau and its surroundings. It removes spatially correlated errors effectively.

'S&W P3M8' uses moving filtering windows [38], whereas the window width w is calculated using:

$$w = \max\left\{ Ae^{-\frac{m}{K}} + 1,\ 5 \right\}, \tag{1}$$

dependent upon the order m of the Stokes coefficients and the parameters (A, K) taking the values (30, 10).

2.3. Computation of Mass Changes from Spherical Harmonic Solutions

We compare all solutions in 24 specially designed mascons for our basins under investigation. While Level-3 mascon solutions only need regridding to align to these 24 basins, the TWS changes from the SH solutions must be calculated first, and then inverted to our mascons. These two computation steps are presented in the following Sections 2.3.1 and 2.3.2, respectively.

2.3.1. Terrestrial Water Storage Changes from Spherical Harmonic Coefficients

The mass change at any time is usually defined with respect to an unchanged earth mass, which can be calculated by the averages of the Stokes coefficients during the observa-

tion time span. The mass change (in equivalent water thickness (EWT)) at any time and at an arbitrary site with co-latitude θ and longitude φ, can be calculated by a synthesis of SH coefficients [40]:

$$\Delta \mathrm{EWT}(\theta,\ \varphi) = \frac{a\rho_{ave}}{3\rho_w} \sum_{l=0}^{lmax} \sum_{m=0}^{l} \frac{2l+1}{1+k_l} \times (\Delta c_{lm} cosm\varphi + \Delta s_{lm} sinm\varphi) \widetilde{P}_{lm}(cos\theta) \quad (2)$$

where Δc_{lm} and Δs_{lm} are the changes in Stokes coefficients from GRACE gravity SH solutions, k_l is the degree l elastic load Love number for potential perturbation [41], $\widetilde{P}_{lm}(cos\theta)$ is the lth degree and mth order normalized associated Legendre polynomial ($lmax = 60$), ρ_{ave} is the average density of the earth (5.517 g/cm^3), ρ_w is the water density (1 g/cm^3), and a is the average radius of the Earth.

If the TWS changes from the SH solutions are simply used to estimate the total TWS change for a region of interest, the results are inevitably affected by signal leakages due to the truncation of higher harmonic degree terms and necessary filtering (e.g., using Gaussian filter [39]) and rescaling. Therefore, we used a mascon fitting treatment (Jacob et al. [42]), which could avoid the problem to a large degree.

2.3.2. Mascon Inverted Terrestrial Water Storage Changes

Following Jacob et al. [42] and Xiang et al. [19], the study area was divided into a total number of $M = 700$ independent mascons, with 14 irregular glacier mascons (see Figure 1) combined with regular $2^\circ \times 2^\circ$ mascons. Each mascon is supposed to be covered by a uniformly distributed unit EWT, which can be decomposed into SH coefficients $\Delta c\prime^i_{lm}$ and $\Delta s\prime^i_{lm}$ (i = 1, 2,..., M) with Equations (4) or (5) by Xiang et al. [16]. According to Jacob et al. [42] and Yi and Sun [8], the mass change in each mascon at any time minimizes the standard least squares merit function using the spectral domain inverse method:

$$min||A^G - Bm||_2^2, \quad (3)$$

where A^G is a group of the changes in Stokes coefficients for a month or the trend of GRACE data during the study time span, and thus rewritten as $(\omega_1\Delta c_{1,0},\ \omega_1\Delta c_{1,1}, \cdots, \omega_l\Delta c_{l,l}, \omega_1\Delta s_{1,1},\ \omega_2\Delta s_{2,1}, \cdots, \omega_l\Delta s_{l,l})^T$, excluding the coefficient for l = 0, with the length of $(l+1)^2 - 1$, which is 3720 for $lmax$ = 60. Smoothing factor ω_l is the degree coefficient of the Jekeli's Gaussian averaging function for Legendre expansion [39]. B is the matrix composed of M columns, with the jth column $B_{.,j} = A^{mas}_j$. A^{mas}_j is a column vector like A^G, but for the Stokes coefficients decomposed from the jth mascon, which also considered ω_l matching with A^G, and rewritten as $\left(\omega_1\Delta c\prime^j_{1,0},\ \omega_1\Delta c\prime^j_{1,1}, \cdots, \omega_l\Delta c\prime^j_{l,l}, \omega_1\Delta s\prime^j_{1,1},\ \omega_2\Delta s\prime^j_{2,1}, \cdots, \omega_l\Delta s\prime^j_{l,l}\right)^T$.

Singularity is always a problem in reverse problems in a geophysical inversion, and regularization is usually applied [8]. The regularized iterative algorithm (RIA) method is one simple and effective regularization approach which has been suggested by Li et al. [43] and Mao and Yang [44]. According to their studies, the RIA method can be expressed as:

$$\left(B^TB + \alpha I\right)m^k = B^TA^G + \alpha m^{k-1}, \quad (4)$$

where α is a nonzero smoothing constant, I is a unit matrix (same order as B^TB), and $k(= 1,\ 2,\ 3,\ \ldots)$ represents the number of iterations. The vector m is supposed to converge to the true solution [44]. The RIA performed very well in a comparison with three other regularization methods [19], and thus was preferred by us here.

Yi and Sun [8] have pointed out that the fitting residue for the regional area is heavily disturbed by the global signals using the spectral domain inverse method with GRACE SH solutions directly. Following Xiang et al. [16], we enlarged the area of concern by 5 degrees

outwards and synthesized the grid TWS changes in these areas, then decomposed them into SH coefficients up to d/o 60, providing A^G used in Equation (4).

3. Results and Discussion

TWS changes from SH solutions using Equation (2) are the intermediate results where we can verify the effectiveness of the destriping filter. This is examined first in Section 3.1.1. After that, the inversion processing frame with the RIA method using Equation (4) is adopted to provide basin-scale inverted TWS change trends and time series at the selected 14 glacier mascons and 10 water basins (Figure 1). We not only investigate the difference in their trends (Section 3.1.2), but also the time series (Section 3.2) of the 24 typical mass change regions to better understand the effects of GRACE solutions on the inverted results.

3.1. Effects on Terrestrial Water Storage Change Trends

In the next section, TWS change trends are first analyzed as derived directly from SH coefficients after application of the destriping filter. Thereafter, in Section 3.1.2, we investigate the effects of GRACE solution selection on the TWS change trends at the mascon level.

3.1.1. Effects on TWS Changes Derived from Spherical Harmonic Coefficients

For a first clear view on spatial details, we do not apply a Gaussian smoothing filter, although omitting it allows high-frequency noises spatially. Figure 2 shows GRACE observed gravity changes and patterns after destriping, representing a visual display and a check of the intermediate results based on which the subsequent mascon inversion processing is performed. So, these TWS change trends in Figure 2 are not the final results due to possible truncation and signal leakage effects and other residual errors in processing.

Figure 2 shows no obvious spatial stripes highlighting the effectiveness of 'S&W P3M8' for the SH solutions. Outside of the TP, we identify four strong negative signals. The first two negative signals are very strong and continuous from Northwest India to the Bengal Basin due to excessive use of groundwater, which merge visually into one signal with the negative signal caused by glacier melting from the Himalayas due to the distance being too close and signal leakage. The third is in the southeast of the TP and is mainly caused by serious glacier melting. The fourth one is in the Tien Shan due to increased ice melting [16,17,45]. A dumbbell-like positive signal is found throughout the northern part of the TP. One signal center is in the eastern TP around the three-rivers source region and the Qaidam Basin, and it is probably the result of an increase in groundwater and soil moisture [16,17]. The other center in the western TP around West Kunlun and Karakoram may be caused by a slight gain in glacier mass.

The TWS change trend signals in Figure 2a–l show similarity in signal patterns and amplitudes. In contrast, more different patterns and amplitudes appear in the TWS change trends derived from mascon solutions (Figure 3m–p), especially the signals in the TP.

3.1.2. Effects on Inverted Terrestrial Water Storage Changes

After inversion with the regularized iterative algorithm method, we obtain the inverted TWS changes for the 12 SH solutions which can also be compared with the four mascon solutions. Figures 3–5 and Tables 2–5 show and list the trends and time series in the TP and its surroundings, from January 2003 to December 2015, based on all 16 tested GRACE solutions. Figure 3 confirms that the inverted TWS change trends generally have high consistency with the corresponding results in Figure 2.

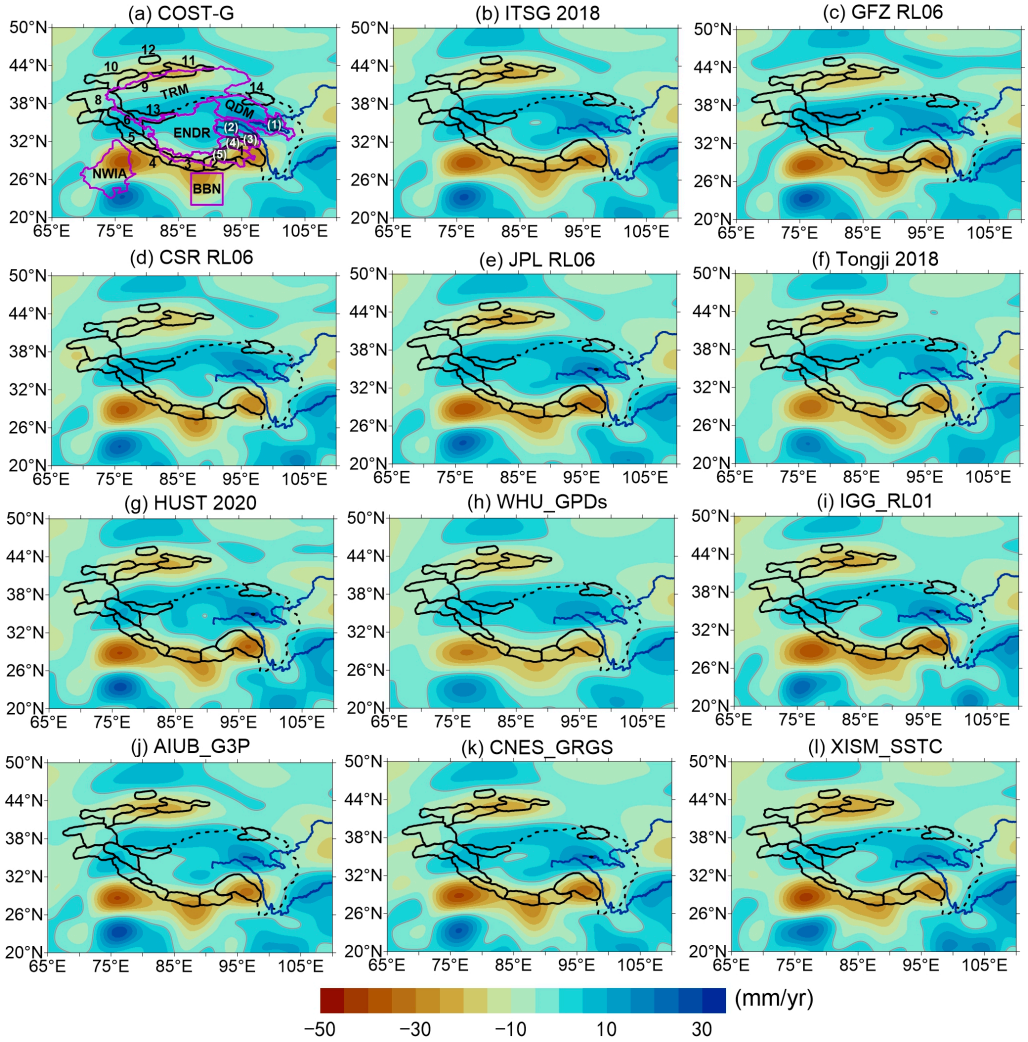

Figure 2. TWS change trends (in mm of EWT/year) from January 2003 to December 2015 from the 12 SH solutions. Destriping filter 'S&W P3M8' with truncation at d/o 60 is used. Note that the trends are without a Gaussian smoothing filter. The 14 black line marked glacier mascons together with the dashed lines delimit the TP and Tien Shan. The blue lines indicate the Yangtze River and the Yellow River, while the gray lines are the 0 contours. In subfigure (**a**), the purple lines, abbreviations and numbers are the same as in Figure 1.

The inverted TWS change trends derived from the GRACE SH solutions (Figure 3a–l) show similar signal patterns with SH synthetic TWS change trends (Figure 2a–l), implying the effectiveness of the SH solutions from different agencies. However, there are also differences in the extent and amplitude of the trend signals. The differences get larger when comparing mascon solutions (Figure 3m–p) for signals inside and outside of the TP. To show the difference quantitatively, we calculate the Pearson's correlation coefficients (PCCs) (upper triangular of Table A1) among inverted TWS change trends in the study areas shown in Figure 3. We find that almost all the PCCs between SH solutions are larger than 0.95 while those PCCs between SH solutions and mascon solutions are all, partly very clearly, smaller than 0.85. Since the most noticeable differences appear in the TP (excluding the glacier melting regions, delimited with the red lines in Figure 3a), we also calculate the PCCs focusing on this area only. The results are listed in the lower triangular area of Table A1. Then, the differences with mascon solutions are even larger. Hence, SH solutions appear to depict the main characteristics of TWS change trends better and more consistently than mascon solutions.

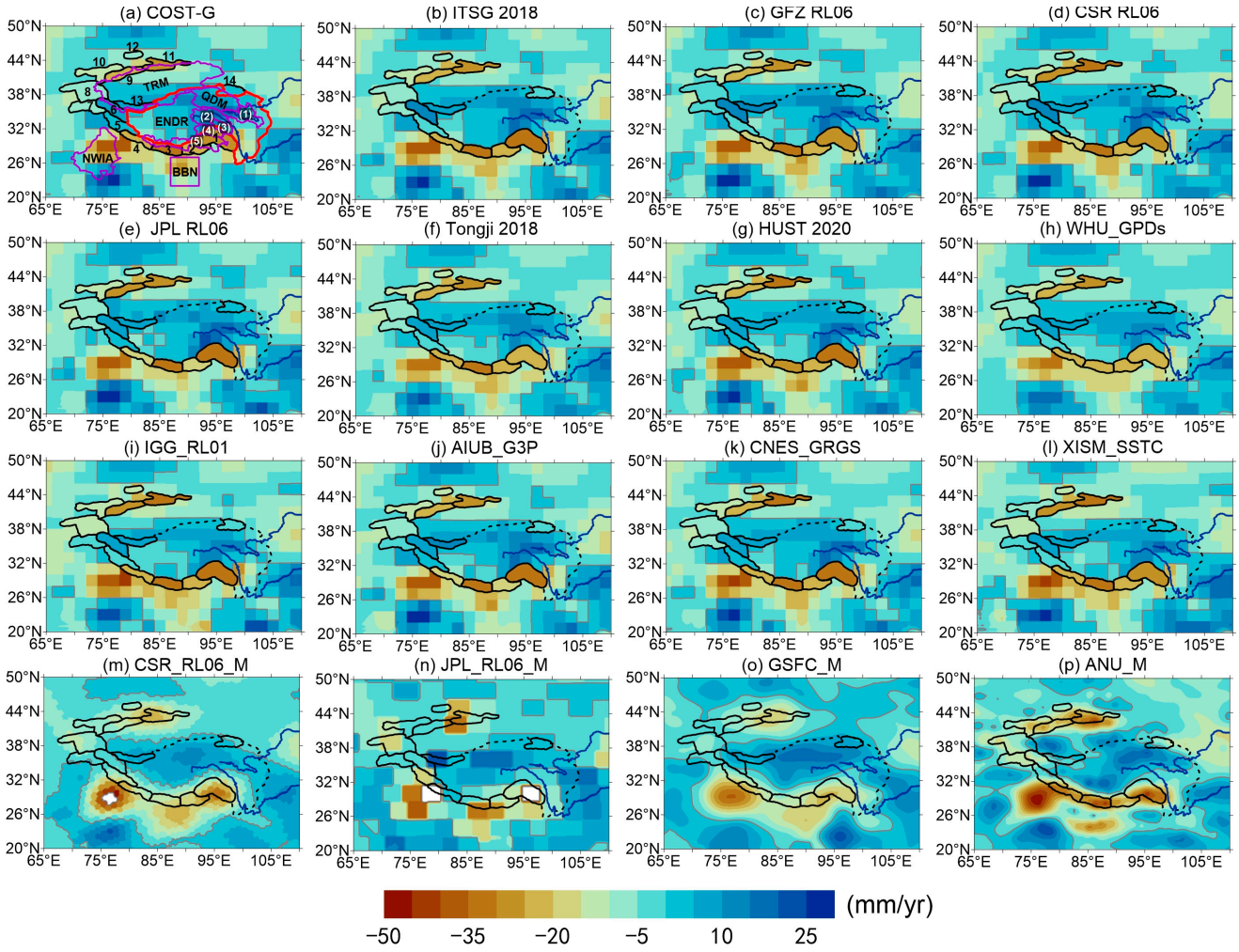

Figure 3. Mascon inverted TWS change trends (in EWT/year) (**a**–**l**) with the regularized iterative algorithm method and (**m**–**p**) as provided by the solution center from January 2003 to December 2015. The subfigures correspond to those in Figure 2, respectively. Note that a 340 km averaging radius Gaussian smoothing filter is used when implementing the inversion for the 12 SH solutions (**a**–**l**). In subfigure (**a**), abbreviations and numbers are the same as in Figure 1. The 14 black line marked glacier mascons together with the dashed lines delimit the TP and Tien Shan. The red lines delimit the inner TP excluding glacier melting regions. The blue lines indicate the Yangtze River and the Yellow River, while the gray lines are the 0 contours.

3.2. Effects on Terrestrial Water Storage Change Time Series

We analyze the features of secular and seasonal signals from the monthly TWS changes for 14 glacier mascons and 10 selected water basins during the period from January 2003 to December 2015. We consider the trend, annual, semiannual, and 161 days aliasing variation (from the S2 semidiurnal solar tide) when implementing a least squares regression analysis on the time series. We use the average from all 16 GRACE solutions as a test benchmark to depict the difference of the time series quantitatively. In addition, we also investigate the difference between the inverted monthly TWS changes with their average derived from 12 SH solutions and between the mascon solutions with their average derived from four mascon solutions. We use PCCs and modified relative root mean square errors (defined by Equation (A2) and simply marked as MRRs here). PCCs and MRRs evaluate the correlation and relative difference between results derived from the GRACE solutions and the test benchmarks. We calculate PCCs both without and with removal of secular trends and

annual amplitudes from the time series. The latter is done to remove large signals that overprint the absolute errors of each time series, and thus may affect the statistics favorably.

The time series of the inverted TWS changes for 14 glacier mascons are shown in Figure 4. The secular trends and annual amplitudes are listed in Table 2, and the two indices are listed in Table 3 (MRRs), Table A2 (PCCs), and Table A3 (PCCs after removal of trend and amplitudes). Similarly, the results for 10 selected water basins are shown in Figure 5, and Tables 4, 5, A4 and A5.

Figure 4 exhibits consistent signals of approximate trends and periodic fluctuations, however, with the difference from each other at every month, displaying the diversity of TWS change estimates due to the GRACE solution selection. Only a few glacier mascons display somewhat disordered time series curves, e.g., Figure 4i,k,m,n. Here, when comparing the three different test benchmarks visually (Figure A1), the average of four mascon solutions (black line) slightly deviates from the other two lines. Despite that, mascon solutions still perform well when considering the errors (Figure A1).

Focusing on the secular trends and annual amplitudes of the time series in Table 2, the trends and amplitudes of TWS changes derived from SH solutions differ less from each other than those from mascon solutions. The latter vary remarkably or yield opposite signs for trend values of certain regions with relatively small or/and controversial trends, which means large divergences between SH solutions and mascon solutions, and between different mascon solutions. For further analysis, we classify these values in four intervals using one, two, and three standard deviations (1-STD, 2-STD, and 3-STD) and above. We can clearly see that most of the significantly deviating secular trends and annual amplitudes concern mascon solutions, implying huge variability and inconsistency of the TWS changes from mascon solutions themselves. One reason for this difference is that the mascon solutions are not aligned with the basins of our studies, whereas the mascon solutions themselves have different spatial resolutions. We recall that we regridded the mascon solutions to align with glacier and water basin mascons.

Combining the results of Figure 4 and Table 2, time series curves with larger trends and amplitudes with obvious periodicity show more consistent features, and vice versa; the differences of time series at every month are more distinct when the trends and amplitudes are small with no apparent regular periodicity (such as Figure 4i,k,m,n). This is an expected result for a time series analysis, which is further supported when looking at PCCs (Table A2). Most of them are over 0.9, showing strong correlations with small differences due to different solutions. This changes after removing the annual amplitudes and secular trends (Table A3). The PCCs become smaller and show more differences between solutions. Compared to the average of all solutions, the PCCs for COST-G and ITSG are generally greater than the PCCs of other solutions (Tables A2 and A3), while, when looking at MRRs (Table 3), the corresponding MRRs for COST-G and ITSG are usually smaller than those of other solutions. That COST-G is close to the mean of all solutions is likely because COST-G is based on a weighted combination of individual SH solutions generated by different agencies [25], where ITSG and CSR hold high weights which are usually larger than 0.5 or even sometimes as large as 0.8 (see Figure A2). Again, we note that the discreteness of the inverted TWS changes derived from different GRACE data is more obvious by MRRs (Table 3) when the annual amplitudes are small with less periodicity for various reasons. This is, for example, the case for the central (mascon 9) and eastern (mascon 11) part of Tien Shan, West Kunlun (mascon 13), and Qilian (mascon 14) (Figure 4i,k,m,n) whose MRRs values are usually much larger. However, there are also other separate cases with large MRRs due to solution differences.

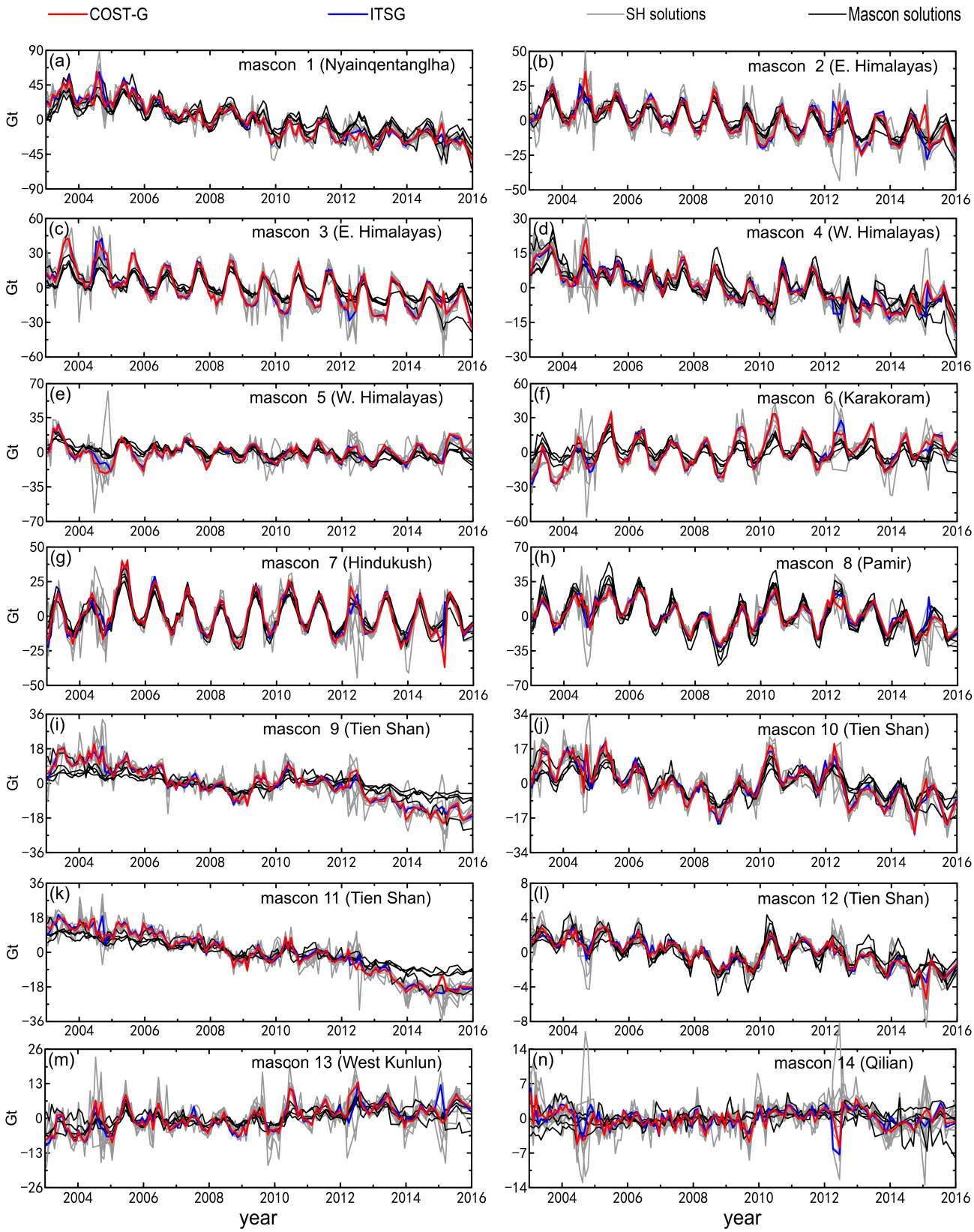

Figure 4. Mascon inverted TWS change time series with the regularized iterative algorithm method (in Gt/year) derived from 16 solutions at 14 glacier mascons (**a**–**n**) from January 2003 to December 2015. Mascon names can be found in each subfigure.

Table 2. Trends and annual amplitudes of inverted TWS changes derived from 16 solutions at 14 glacier mascons. Units are in Gt/year for trends and in Gt for annual amplitude. The 'AVE' column in green represents average of all 16 values, while the 'STD' column in light green is the standard deviation. Values within the 1-STD (one standard deviation) bounds are in black, within the 2-STD (two standard deviations) bounds in blue, within the 3-STD (three standard deviations) bounds in red, and above that in purple and bold.

No.	Mascon	Secular Trends																	
		COST-G	ITSG	GFZ	CSR	JPL	Tongji	HUST	WHU	IGG	AIUB	GRGS	XISM	CSR_M	JPL_M	GSFC_M	ANU_M	AVE	STD
1	Nyainqentanglha	−5.85	−6.06	−5.85	−5.82	−6.26	−4.82	−6.03	−4.52	−6.09	−5.98	−5.98	−5.32	−4.24	−5.54	−3.01	−4.45	−5.36	0.88
2	E. Himalayas	−1.87	−1.99	−1.91	−2.08	−1.70	−1.92	−2.04	−1.98	−2.09	−1.71	−1.96	−1.91	−1.77	−1.36	−1.60	−2.18	−1.88	0.20
3		−2.87	−2.98	−3.03	−2.93	−3.06	−2.86	−2.71	−2.25	−3.16	−2.95	−3.06	−3.04	−1.37	−1.40	−1.09	−3.06	−2.61	0.67
4	W. Himalayas	−1.55	−1.59	−1.40	−1.44	−1.44	−1.57	−1.68	−1.66	−1.65	−1.49	−1.77	−1.57	−1.20	−1.51	−1.26	−2.22	−1.56	0.22
5		0.03	−0.09	−0.05	0.10	0.02	−0.48	0.21	−0.22	−0.22	0.13	0.10	−0.20	−1.08	−1.29	−0.96	−0.85	−0.30	0.47
6	Karakoram	1.11	1.20	1.19	1.16	0.82	0.88	1.06	0.95	1.08	0.98	0.90	0.97	−0.19	−0.18	0.28	−0.88	0.71	0.60
7	Hindukush	−0.65	−0.50	−0.47	−0.48	−0.77	−0.57	−0.55	−0.23	−0.24	−0.41	−0.70	−0.19	−0.24	−0.12	−0.12	−1.11	−0.46	0.26
8	Pamir	−1.25	−1.02	−0.69	−1.47	−1.10	−1.16	−1.23	−1.18	−1.94	−1.06	−1.35	−0.21	−1.41	−1.86	−0.81	−1.36	−1.19	0.40
9		−2.07	−2.02	−1.98	−2.16	−2.21	−2.09	−2.04	−1.98	−2.21	−1.90	−2.09	−2.26	−1.04	−0.63	−0.78	−1.93	−1.84	0.51
10	Tien Shan	−1.26	−1.26	−1.16	−1.25	−1.30	−1.46	−1.37	−1.25	−1.20	−1.21	−1.25	−1.09	−0.81	−0.52	−0.47	−1.70	−1.16	0.31
11		−2.74	−2.80	−2.56	−2.88	−2.66	−2.71	−2.88	−2.45	−2.88	−2.77	−2.96	−2.97	−1.77	−1.69	−1.40	−2.43	−2.53	0.47
12		−0.29	−0.29	−0.27	−0.26	−0.24	−0.33	−0.30	−0.26	−0.34	−0.31	−0.28	−0.37	−0.29	−0.17	−0.21	−0.27	−0.28	0.05
13	West Kunlun	0.65	0.76	0.85	0.62	0.63	0.67	0.45	0.66	0.61	0.85	0.63	0.49	0.39	0.89	0.60	**−0.08**	0.60	0.22
14	Qilian	0.01	−0.03	0.07	0.07	0.01	0.12	0.05	0.12	−0.18	−0.10	−0.07	0.03	0.03	0.13	0.45	−0.33	0.02	0.16
No.	**Mascon**	**Annual Amplitudes**																	
		COST-G	ITSG	GFZ	CSR	JPL	Tongji	HUST	WHU	IGG	AIUB	GRGS	XISM	CSR_M	JPL_M	GSFC_M	ANU_M	AVE	STD
1	Nyainqentanglha	8.52	9.39	9.14	8.81	10.62	9.35	9.32	9.99	9.31	8.58	8.51	8.44	11.69	**20.55**	11.31	8.30	10.11	2.87
2	E. Himalayas	11.05	11.40	10.70	11.36	10.42	13.48	11.55	15.20	12.36	11.30	9.78	9.21	9.00	11.15	9.10	5.58	10.79	2.06
3		15.84	16.26	16.22	15.74	17.42	17.27	14.52	17.40	17.02	15.92	15.73	14.02	8.91	9.64	8.12	8.05	14.26	3.36
4	W. Himalayas	4.01	3.98	3.46	3.87	3.66	3.13	3.97	4.10	4.10	4.45	4.12	3.05	3.71	5.40	3.27	2.22	3.78	0.68
5		8.90	8.66	8.96	8.89	4.70	7.23	9.05	5.45	8.25	8.71	9.62	9.63	4.77	2.32	4.63	6.72	7.28	2.17
6	Karakoram	14.58	14.54	14.49	14.53	12.93	13.28	15.15	11.03	13.08	15.10	14.52	14.03	8.78	4.01	9.24	9.60	12.43	3.01
7	Hindukush	16.09	15.76	16.27	16.52	15.10	14.01	16.01	11.84	14.87	16.25	16.08	14.52	12.23	15.77	12.13	13.92	14.84	1.54
8	Pamir	12.69	13.13	14.62	12.43	12.77	14.26	12.27	14.57	12.39	13.05	12.67	11.18	18.00	23.66	16.47	19.17	14.58	3.16
9		3.43	3.25	2.89	3.46	3.12	2.81	3.41	2.19	3.21	3.81	2.75	2.07	1.78	1.06	1.83	1.17	2.64	0.82
10	Tien Shan	6.43	6.34	6.26	7.00	7.19	5.87	6.16	5.73	5.70	6.58	6.71	4.63	5.41	3.90	5.52	5.31	5.92	0.83
11		2.36	2.30	3.37	2.25	2.46	3.05	2.26	2.76	1.83	2.63	2.08	1.89	0.81	1.23	1.81	2.46	2.22	0.61
12		0.92	0.91	1.19	0.98	1.14	0.94	0.95	0.86	0.90	0.96	0.89	0.99	1.21	0.71	1.43	**1.84**	1.05	0.26
13	West Kunlun	3.76	3.49	3.64	3.74	4.36	4.18	3.66	4.19	3.62	4.25	3.42	2.80	1.59	1.86	2.11	0.89	3.22	1.02
14	Qilian	0.74	0.70	0.91	1.09	0.60	0.52	0.60	0.34	0.59	1.10	0.35	1.40	0.23	0.60	0.27	1.45	0.72	0.37

Table 3. Modified relative root mean square errors (MRRs) between the average of all 16 GRACE solutions (MRR1) and 12 SH solutions (for SH solutions) or four mascon solutions (for mascons) (MRR2) and TWS change time series at 14 glacier mascons derived from each of the 16 different GRACE SH solutions.

No.	Mascon	COST-G		ITSG		GFZ		CSR		JPL		Tongji		HUST		WHU	
		MRR1	MRR2	MRR1	MRR2	MRR1	MRR2	MRR1	MRR2	MRR1	MRR2	MRR1	MRR2	MRR1	MRR2	MRR1	MRR2
1	Nyainqentanglha	0.42	0.33	0.43	0.38	0.47	0.44	0.65	0.60	0.89	0.91	0.60	0.70	0.67	0.63	0.62	0.83
2	E. Himalayas	0.32	0.27	0.30	0.28	0.28	0.25	0.54	0.51	0.62	0.56	0.43	0.37	0.46	0.41	0.50	0.44
3		0.23	0.17	0.27	0.21	0.28	0.21	0.35	0.28	0.66	0.55	0.33	0.28	0.42	0.36	0.31	0.29
4	W. Himalayas	0.49	0.40	0.40	0.37	0.74	0.70	1.13	1.03	0.94	0.85	0.65	0.67	0.79	0.77	0.55	0.65
5		0.40	0.27	0.32	0.25	0.54	0.43	0.61	0.46	1.66	1.46	0.45	0.46	0.69	0.53	0.46	0.49
6	Karakoram	0.25	0.13	0.28	0.17	0.33	0.22	0.36	0.26	0.79	0.68	0.35	0.32	0.48	0.39	0.28	0.32
7	Hindukush	0.26	0.25	0.20	0.18	0.28	0.26	0.33	0.31	0.57	0.54	0.24	0.24	0.29	0.28	0.29	0.32
8	Pamir	0.20	0.18	0.26	0.28	0.51	0.56	0.44	0.47	0.43	0.45	0.26	0.32	0.36	0.38	0.21	0.29
9		0.68	0.39	0.68	0.53	1.52	1.25	1.22	0.90	1.72	1.35	0.81	0.67	1.28	1.01	0.74	0.74
10	Tien Shan	0.38	0.30	0.37	0.32	0.80	0.72	0.59	0.52	0.61	0.53	0.50	0.50	0.56	0.51	0.35	0.40
11		0.82	0.63	0.85	0.63	1.13	0.99	1.72	1.34	1.39	1.15	1.22	1.05	1.59	1.24	0.90	0.94
12		0.31	0.26	0.32	0.32	0.83	0.86	0.55	0.57	0.70	0.76	0.50	0.51	0.62	0.64	0.39	0.48
13	West Kunlun	0.45	0.34	0.56	0.46	0.94	0.77	0.77	0.63	1.66	1.35	0.53	0.44	1.01	0.84	0.61	0.53
14	Qilian	1.68	1.21	2.23	1.82	3.70	2.97	4.49	3.44	3.48	2.79	2.42	2.09	4.96	4.04	2.46	2.30
No.	**Mascon**	**IGG**		**AIUB**		**GRGS**		**XISM**		**CSR_M**		**JPL_M**		**GSFC_M**		**ANU_M**	
		MRR1	MRR2	MRR1	MRR2	MRR1	MRR2	MRR1	MRR2	MRR1	MRR2	MRR1	MRR2	MRR1	MRR2	MRR1	MRR2
1	Nyainqentanglha	0.66	0.68	0.74	0.71	0.55	0.52	0.87	0.89	0.67	0.16	1.12	0.71	1.00	0.44	0.78	0.55
2	E. Himalayas	0.46	0.41	0.39	0.35	0.31	0.28	0.51	0.49	0.32	0.12	0.37	0.30	0.33	0.18	0.49	0.43
3		0.42	0.33	0.38	0.32	0.26	0.20	0.41	0.36	0.46	0.23	0.45	0.31	0.52	0.31	0.48	0.69
4	W. Himalayas	0.85	0.77	0.81	0.76	0.67	0.61	0.99	0.94	0.66	0.49	1.02	0.68	0.67	0.43	1.01	0.91
5		0.63	0.55	0.57	0.43	0.58	0.43	0.81	0.69	0.65	0.27	0.84	0.61	0.63	0.30	0.54	0.64
6	Karakoram	0.33	0.26	0.51	0.42	0.30	0.22	0.42	0.35	0.46	0.19	0.68	0.45	0.39	0.34	0.60	0.48
7	Hindukush	0.32	0.30	0.33	0.30	0.24	0.22	0.47	0.44	0.24	0.13	0.25	0.24	0.27	0.18	0.29	0.26
8	Pamir	0.42	0.44	0.46	0.49	0.43	0.46	0.52	0.53	0.32	0.11	0.64	0.29	0.31	0.22	0.42	0.22
9		1.11	0.83	1.39	1.12	0.86	0.66	1.79	1.42	1.39	0.68	1.99	1.49	1.69	1.31	1.41	2.87
10	Tien Shan	0.57	0.52	0.57	0.52	0.47	0.42	0.75	0.70	0.48	0.19	0.67	0.38	0.63	0.42	0.65	0.76
11		1.62	1.27	1.43	1.18	1.19	0.86	1.98	1.57	1.68	0.84	1.83	1.07	2.18	1.70	1.50	2.87
12		0.63	0.66	0.62	0.64	0.47	0.51	0.79	0.86	0.42	0.27	0.58	0.44	0.56	0.32	1.00	0.62
13	West Kunlun	0.94	0.76	1.15	0.92	0.57	0.48	1.13	0.95	0.64	0.53	0.78	1.44	0.55	0.94	1.25	1.89
14	Qilian	4.18	3.24	5.61	4.55	2.80	2.34	4.80	3.73	2.16	2.36	2.63	3.19	3.84	7.00	4.43	9.67

For the 10 selected water basins, the time series with stable signal periods and large amplitudes show very good agreement and small differences between the time series from different solutions, i.e., Northwest India (NWIA), Bengal Basin (BBN), and Yarlung Zangbo River Basin (YZBR) (Figure 5a,b,j, respectively). However, for the Tarim Basin

(TRM) and other basin areas with weak TWS change signals with small amplitudes, trends and/or no stable signal periods in the TP, the difference is more obvious. This is the case for the Qaidam Basin (QDM), Endorheic Region of the TP (ENDR), Yellow River source region (YLRS), Yangtze River source region (YZRS), Mekong River source region (MKRS), Salween River source region (SWRS), and Yarlung Zangbo River Basin (YZBR) (Figure 5c–i). Looking at Figure A3, the comparison of the three solution averages also exhibits larger deviations for the average from four mascon solutions (black line) for basin areas with weak TWS change signals, although they agree well within errors. An inspection of the secular trends and annual amplitudes in Table 4 shows that most of the larger deviating trends and annual amplitudes are found for the four mascon solutions. In addition, larger differences appear between SH solutions and mascon solutions and between different mascon solutions, mirroring the performance in glacier mascon regions. We recall, however, that mascon solutions were regridded to align with the glacier and water basin mascons of our study. According to Tables 5, A4 and A5, again, the COST-G and ITSG are closest to the average of all solutions and have smaller MRRs than others. This is especially the case when considering all basins including smaller ones. However, we note that the difference between PCCs without and with removal of trends and amplitudes is not as large as that for the glacier basins.

Larger MRRs appear along with time series with small amplitudes and less periodicity. Therefore, in the TP and its surroundings, the effects of GRACE solutions on inverted terrestrial water storage changes are more pronounced when the signals are weak and amplitudes are small with no stable signal periods, while the effects are relatively weak when the signals are strong with stable periods. However, this behavior is expected for a time series.

Table 4. Trends and annual amplitudes of inverted TWS changes derived from 16 solutions at 10 selected water basins. Units are in Gt/year for trends and in Gt for annual amplitude. The 'AVE' column in green represents average of all 16 values, while the 'STD' column in light green is the standard deviation. Values within the 1-STD (one standard deviation) bounds are in black, within the 2-STD (two standard deviations) bounds in blue, within the 3-STD (three standard deviations) bounds in red, and above that in purple and bold.

Area	Secular Trend																
	COST-G	ITSG	GFZ	CSR	JPL	Tongji	HUST	WHU	IGG	AIUB	GRGS	XISM	CSR_M	JPL_M	GSFC_M	ANU_M	AVE	STD
NWIA	−6.07	−5.79	−5.80	−5.85	−5.03	−5.86	−6.44	−5.23	−6.87	−5.77	−6.47	−6.46	−7.50	−8.07	−5.97	−8.47	−6.35	0.96
BBN	−4.71	−4.43	−4.73	−4.60	**−2.92**	−4.62	−4.74	−3.97	−4.61	−4.51	−4.50	−4.23	−4.35	−4.34	−4.32	−3.57	−4.32	0.48
TRM	−2.39	−2.08	−1.31	−2.11	−1.02	−2.81	−2.68	−2.52	−4.31	−1.98	−2.52	−5.38	−3.49	−3.31	−1.16	−3.48	−2.66	1.15
QDM	2.20	2.27	2.44	2.21	1.82	2.09	2.11	1.85	1.83	2.18	1.97	2.11	1.63	1.82	3.09	2.71	2.15	0.37
ENDR	1.68	1.67	1.75	1.52	2.18	0.95	1.10	1.35	0.83	1.85	1.43	0.86	3.20	4.59	5.21	4.24	2.15	1.39
YLRS	0.79	0.82	0.96	0.76	0.89	0.63	0.83	0.52	0.81	0.72	0.71	1.07	0.53	0.51	0.64	0.29	0.72	0.19
YZRS	1.70	1.70	1.62	1.66	1.57	1.31	1.65	1.42	1.41	1.67	1.61	1.42	0.58	0.51	1.19	0.79	1.36	0.40
MKRS	0.20	0.22	0.21	0.23	0.22	0.12	0.20	0.15	0.16	0.21	0.22	0.17	−0.44	−0.37	−0.24	−0.12	0.07	0.23
SWRS	−0.96	−1.01	−0.95	−0.90	−0.75	−0.83	−0.98	−0.73	−1.04	−1.00	−0.97	−0.86	−0.89	−1.03	−0.51	−0.46	−0.87	0.18
YZBR	−4.36	−4.50	−4.33	−4.47	−3.43	−4.17	−4.53	−3.92	−4.56	−4.30	−4.51	−4.09	−4.27	−3.06	−3.43	−5.14	−4.19	0.52

Area	Annual Amplitudes																
	COST-G	ITSG	GFZ	CSR	JPL	Tongji	HUST	WHU	IGG	AIUB	GRGS	XISM	CSR_M	JPL_M	GSFC_M	ANU_M	AVE	STD
NWIA	23.22	22.74	22.18	22.08	21.04	24.77	23.34	25.30	23.49	23.82	23.00	20.76	30.20	36.45	31.50	24.48	24.90	4.24
BBN	76.98	76.26	76.53	77.32	67.07	73.23	76.78	68.02	75.79	77.52	75.79	69.30	72.41	69.46	65.52	64.75	72.67	4.60
TRM	15.44	15.02	17.12	15.59	15.21	17.26	14.50	15.79	12.82	14.08	14.09	14.02	9.54	12.00	17.94	19.16	14.97	2.36
QDM	2.07	2.27	2.17	2.21	1.49	2.06	2.25	3.69	2.18	2.18	1.92	5.57	2.67	4.29	2.29	4.13	2.72	1.10
ENDR	13.92	15.38	14.60	16.31	13.21	16.30	17.53	17.40	15.53	14.81	10.78	2.38	12.76	11.58	7.89	5.37	12.86	4.35
YLRS	1.31	1.34	1.08	1.47	1.02	1.02	1.16	1.88	0.67	1.53	1.95	2.60	3.71	1.86	3.74	2.57	1.81	0.92
YZRS	5.71	5.78	5.39	6.20	5.46	4.84	5.75	4.85	5.56	5.33	5.38	4.51	3.33	2.13	2.04	2.70	4.69	1.36
MKRS	2.08	2.09	2.13	2.20	2.12	1.31	1.77	0.97	2.11	2.19	1.96	1.83	1.45	1.14	1.33	0.36	1.69	0.54
SWRS	1.56	1.91	1.51	1.60	1.78	1.61	1.94	2.00	1.74	1.72	1.20	0.21	2.08	**4.15**	1.76	0.88	1.73	0.80
YZBR	12.50	13.46	12.44	12.99	11.95	15.23	13.81	17.75	14.03	13.12	10.98	8.67	13.94	14.29	12.94	5.93	12.75	2.65

Table 5. Similar to Table 3, but showing the results for the MRRs at 10 selected water basins.

Area	COST-G		ITSG		GFZ		CSR		JPL		Tongji		HUST		WHU	
	MRR1	MRR2	MRR1	MRR2	MRR1	MRR2	MRR1	MRR2	MRR1	MRR2	MRR1	MRR2	MRR1	MRR2	MRR1	MRR2
NWIA	0.13	0.12	0.20	0.20	0.18	0.16	0.28	0.26	0.28	0.26	0.20	0.21	0.24	0.26	0.27	0.26
BBN	0.06	0.05	0.07	0.06	0.07	0.06	0.10	0.09	0.19	0.18	0.07	0.07	0.10	0.09	0.10	0.10
TRM	0.35	0.30	0.51	0.44	0.66	0.58	0.62	0.56	0.79	0.73	0.73	0.66	0.55	0.50	0.48	0.43
QDM	0.65	0.50	0.99	0.83	1.46	1.19	1.63	1.31	1.37	1.16	1.71	1.47	1.77	1.43	1.57	1.39
ENDR	0.34	0.23	0.48	0.35	0.47	0.38	0.74	0.57	0.70	0.61	0.77	0.57	0.72	0.50	0.63	0.44
YLRS	1.29	1.08	1.48	1.36	2.25	2.09	2.34	2.51	2.24	2.30	1.70	1.85	2.39	2.37	1.63	2.22
YZRS	0.47	0.29	0.49	0.31	0.43	0.30	0.78	0.61	0.79	0.58	0.52	0.48	0.77	0.58	0.48	0.42
MKRS	0.60	0.31	0.72	0.46	0.83	0.52	1.25	0.87	1.96	1.39	0.78	0.69	1.45	1.05	0.72	0.72
SWRS	0.69	0.50	0.70	0.61	0.84	0.79	1.17	1.04	1.02	1.04	1.12	1.11	0.99	0.89	0.85	0.98
YZBR	0.21	0.17	0.21	0.19	0.21	0.20	0.38	0.34	0.39	0.38	0.29	0.27	0.29	0.25	0.46	0.42
Area	**IGG**		**AIUB**		**GRGS**		**XISM**		**CSR_M**		**JPL_M**		**GSFC_M**		**ANU_M**	
	MRR1	MRR2	MRR1	MRR2	MRR1	MRR2	MRR1	MRR2	MRR1	MRR2	MRR1	MRR2	MRR1	MRR2	MRR1	MRR2
NWIA	0.35	0.37	0.24	0.25	0.23	0.24	0.43	0.42	0.37	0.16	0.55	0.25	0.32	0.26	0.49	0.35
BBN	0.17	0.17	0.11	0.10	0.07	0.07	0.17	0.17	0.10	0.08	0.12	0.08	0.11	0.08	0.15	0.10
TRM	0.84	0.78	0.92	0.83	0.72	0.64	1.23	1.19	0.47	0.58	0.55	0.68	0.81	1.08	1.58	1.58
QDM	1.92	1.55	2.02	1.65	1.62	1.32	3.40	2.77	1.78	2.15	2.17	2.31	2.48	2.63	3.37	3.89
ENDR	0.81	0.60	0.84	0.70	0.68	0.57	1.10	0.99	0.58	1.15	0.90	0.90	1.07	1.00	1.58	1.89
YLRS	2.08	2.26	1.94	2.08	2.05	2.00	3.67	3.75	2.46	0.48	2.05	0.51	2.49	0.67	3.37	1.01
YZRS	0.55	0.45	0.99	0.80	0.54	0.40	0.83	0.70	0.89	0.80	0.98	0.69	0.64	1.07	1.08	1.60
MKRS	1.11	0.80	1.16	0.80	0.84	0.57	1.39	0.99	1.67	0.84	1.60	0.69	1.45	0.75	1.26	1.57
SWRS	1.21	1.23	1.10	1.00	0.90	0.81	1.42	1.44	0.96	0.43	1.67	1.06	1.27	0.60	1.84	1.10
YZBR	0.36	0.34	0.33	0.31	0.31	0.28	0.48	0.48	0.28	0.26	0.47	0.39	0.36	0.30	0.68	0.65

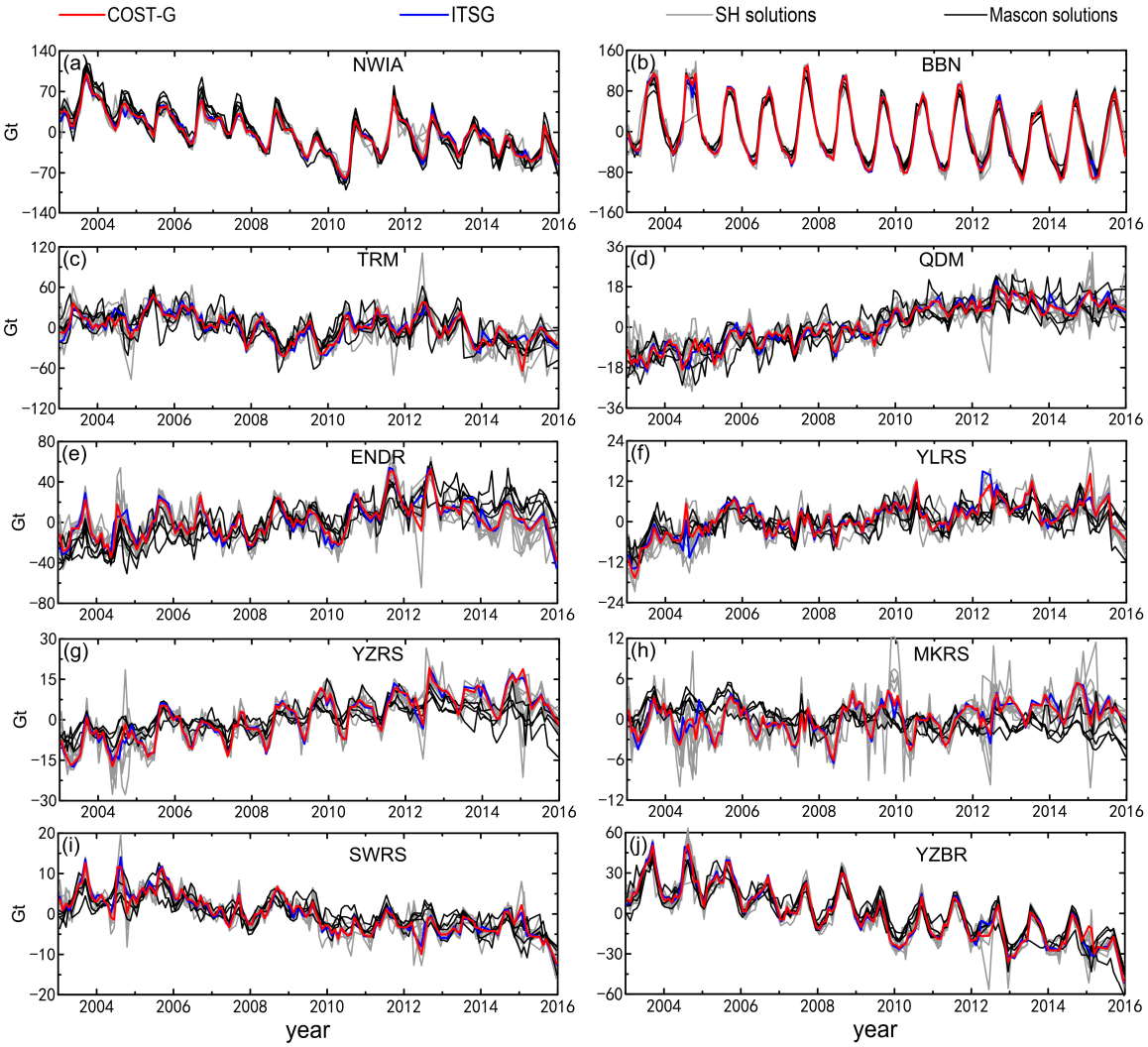

Figure 5. Similar to Figure 4, but showing results for 10 selected water basins: (**a**) NWIA, Northwest India; (**b**) BBN, Bengal Basin; (**c**) TRM, Tarim Basin; (**d**) QDM, Qaidam Basin; (**e**) ENDR, Endorheic

Region of the TP; (**f**) YLRS, Yellow River source region; (**g**) YZRS, Yangtze River source Region; (**h**) MKRS, Mekong River source region; (**i**) SWRS, Salween River source region; (**j**) YZBR Yarlung Zangbo River Basin.

4. Conclusions

In this study, we compared terrestrial water storage (TWS) changes in the Tibetan Plateau (TP) and its surroundings during the period between January 2003 and December 2015 from 16 different GRACE solutions that are classified into 12 spherical harmonic (SH) solutions and four mascon solutions. Differences in trends and time series of the TWS changes exist due to different strategies by different agencies when producing GRACE solutions.

Comparing trends, different SH solutions match well among each other, while there are clear visual differences, especially in the TP, when comparing SH solutions with mascon solutions. When investigating the time series results compared to their averaged result, the COST-G and ITSG SH solutions agree best with the average of all solutions than other SH and all mascon solutions. This is especially the case when secular trends and annual amplitudes are removed before the comparison. The SH solutions lead to different results in the TP and in some glacier mascons where small TWS changes are accompanied with small amplitudes, trends, and/or no stable signal periods. Then, the difference is even larger comparing SH solutions and mascon solutions or between different mascon solutions. In turn, time series usually match each other when the mass change signals are strong with a large amplitude and regular periodicity. This behavior can be expected because any error due to the processing strategy can be significantly overprinted by a strong signal, thus, the apparent error of the time series is lower.

A user certainly wishes to avoid any differences in results that relate to the selection of a GRACE solution. This study is intended to raise a topical discussion on the effect of selecting certain GRACE solutions on TWS changes. Based on the comparison we provide here, the SH solutions of COST-G and ITSG seem preferable for areas with complicated hydrological conditions and where TWS change signals are not distinct in distribution (single and strong signal) and of certain periodicity. Nonetheless, other SH solutions are still performing well as their differences are mostly within one standard deviation only. Hence, a certain SH solution should not be disregarded right away. On another note, the statistical performance of the COST-G SH solution compared to an average of all solutions implies that combined GRACE solutions are an opportunity to develop GRACE products and results further by taking advantage of the best of each solution. However, additional investigations are needed to confirm this implication.

The results from the four mascon solutions studied here were all partly very different (often two standard deviations) from the average of all solutions, even though they can still be considered feasible based on the error statistics (see Figures A1 and A3). Of course, the differences can, to a large part, be related to the fact that we had to regrid the solutions to match our mascons, which would consequently introduce error. However, this makes mascon solutions somewhat less attractive for detailed TWS investigations in the TP and its surroundings.

Based on our preliminary analysis here, we recommend appropriate, i.e., targeted, mascon setting and usage of, if available, combined SH solutions in future GRACE studies on TWS changes in the TP and adjacent areas. Especially, careful setting of known mass change distribution (such as the glacier mascons) appears more suitable for the special situation of the TP.

Author Contributions: Conceptualization, L.X.; methodology, L.X.; software, L.X.; validation, L.X. and H.S.; formal analysis, L.X., H.W., and H.S.; investigation, L.X. resources, L.X., H.W., and H.S.; data curation, L.X.; writing—original draft preparation, L.X.; writing—review and editing, L.X., H.W., and H.S.; visualization, L.X. and H.S.; supervision, L.X., H.W., and H.S.; project administration, L.X.; funding acquisition, L.X. and H.W. All authors have read and agreed to the published version of the manuscript.

Funding: This research was funded by the National Natural Science Foundation of China (42004007, 41974009, and 42374045).

Data Availability Statement: GRACE SH solutions are available on the website of the International Centre for Global Earth Models (ICGEM) (http://icgem.gfzpotsdam.de/series, accessed on 17 April 2023). Degree-1 and C20 data are available via GRACE TN-13 (GRACE Technical Note 13, https://podaac.jpl.nasa.gov/gravity/grace-documentation, accessed on 17 April 2023) and GRACE TN-14 (NASA GSFC SLR C20 and C30 solutions, https://podaac.jpl.nasa.gov/gravity/grace-documentation, accessed on 17 April 2023), respectively. The ICE-6G_C model is available at http://www.atmosp.physics.utoronto.ca/~peltier/data.php, accessed on 8 January 2023.

Acknowledgments: We thank three anonymous reviewers and the academic editor for their careful reading and insightful comments and suggestions, which helped us to improve the manuscript. We are grateful to the agencies that provided the GRACE solutions used in this paper.

Conflicts of Interest: The authors declare no conflict of interest.

Appendix A

Appendix A.1. PCC Value and MRR Value

Pearson's correlation coefficient (PCC) is one of the methods widely used for evaluating the strength of the relationship between two vectors [46]. In addition, we also defined an index of modified relative root mean square errors (MRRMSE, simply marked as MRR) based on Equation (60) of Despotovic et al. [47] to evaluate the relative size of the difference between two vectors. The two indexes of PCC and MRR can be expressed with Equation (A1) and Equation (A2), respectively:

$$\mathrm{PCC} = \frac{cov(\mathrm{TWS},\ \mathrm{BM})}{\sqrt{var(\mathrm{TWS}) \times var(\mathrm{BM})}} \tag{A1}$$

and

$$\mathrm{MRR} = \frac{\sqrt{\frac{\sum_{i=1}^{n}(\mathrm{TWS}_i - \mathrm{BM}_i)^2}{N}}}{A_{\mathrm{BM}}} \tag{A2}$$

where $cov(\mathrm{TWS},\ \mathrm{BM})$ is the covariance of trends on grids of TWS changes and the counterparts of benchmark (BM), or the time series of TWS changes and the benchmark at 24 selected regions; $var(\mathrm{TWS})$ and $var(\mathrm{BM})$ are the corresponding variance, respectively. A_{BM} is the annual amplitude of the benchmark time series.

The PCC values are between -1 and 1, indicating the degree of association between the two variables, the closer the absolute value is to 1, the better the correlation, while the + (plus) and $-$ (minus) sign indicates a positive and negative relationship. The MRR values reflect the relative size relationship between the root mean square errors and the annual amplitude, which is modified from Equation (60) of Despotovic et al. [47] whose denominator is the sum of measured values. However, as we had removed the average of Stokes coefficients to obtain their changes before inversion, this leads to ineffectiveness of their sum as a denominator. Thus, we assigned the annual amplitude to the denominator and obtained Equation (A2) for the MRR. The MRR indicates the relative accuracy of the results [47,48].

Appendix A.2. Complementary Figures and Tables

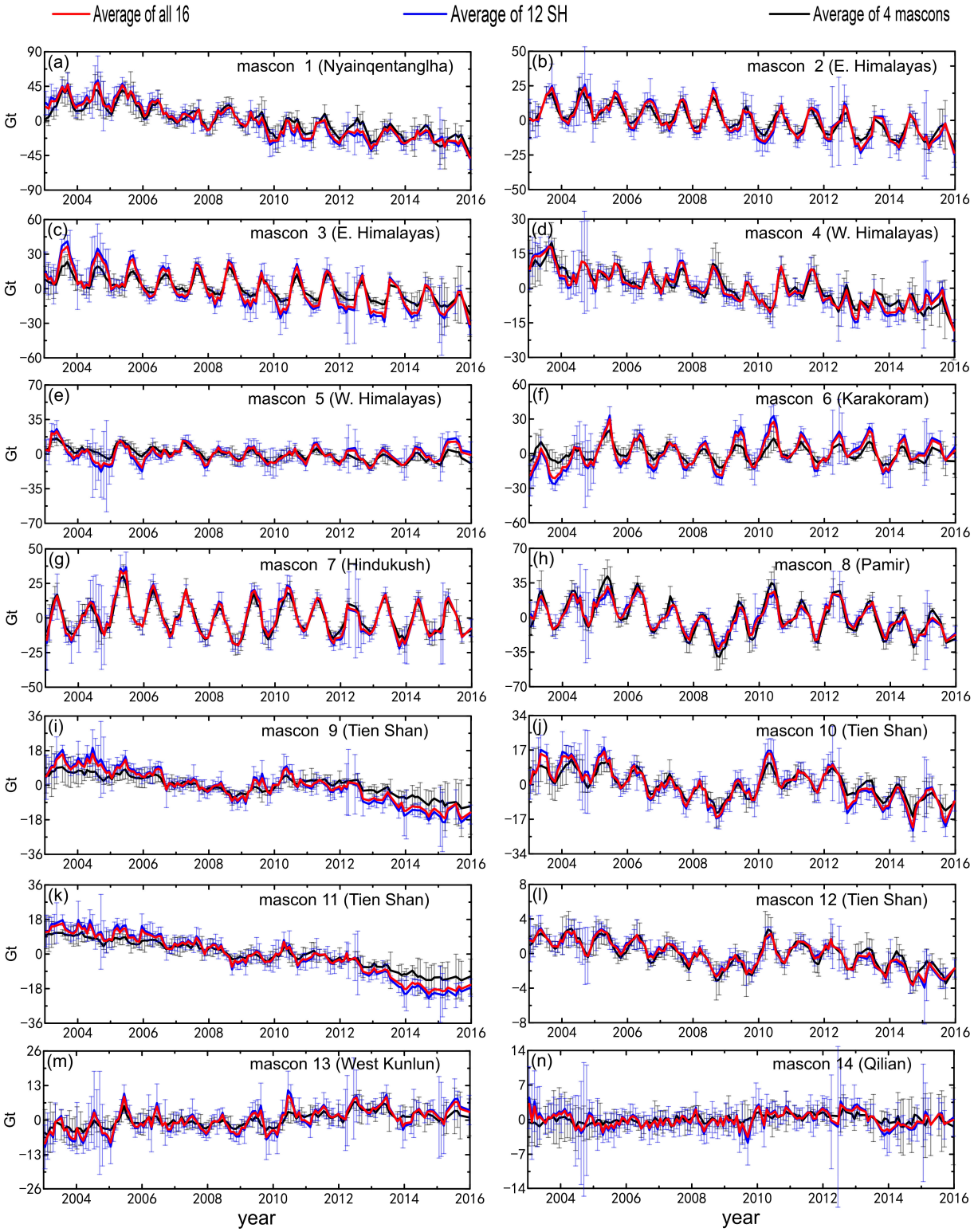

Figure A1. Average time series of the TWS changes derived from 16 GRACE solutions, 12 SH solutions and four mascon solutions, at the 14 glacier mascons (**a**–**n**). Names can be found in each subfigure. Note that the error bars are twice the root mean squared errors. For clarity, we do not show error bars for the red line.

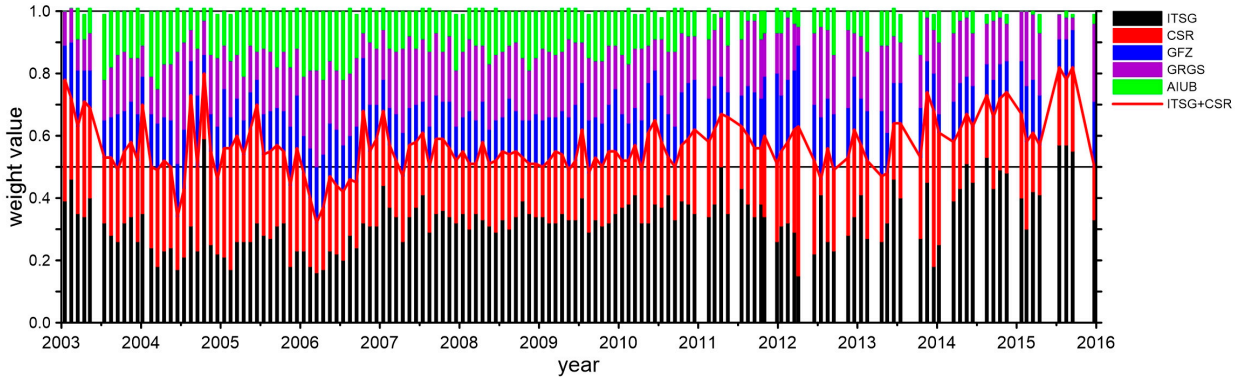

Figure A2. Weight values imposed on monthly Stokes coefficients of different GRACE SH solutions for producing the COST-G solution. The color bars indicate different weight values which add up to 1.0 for each single month.

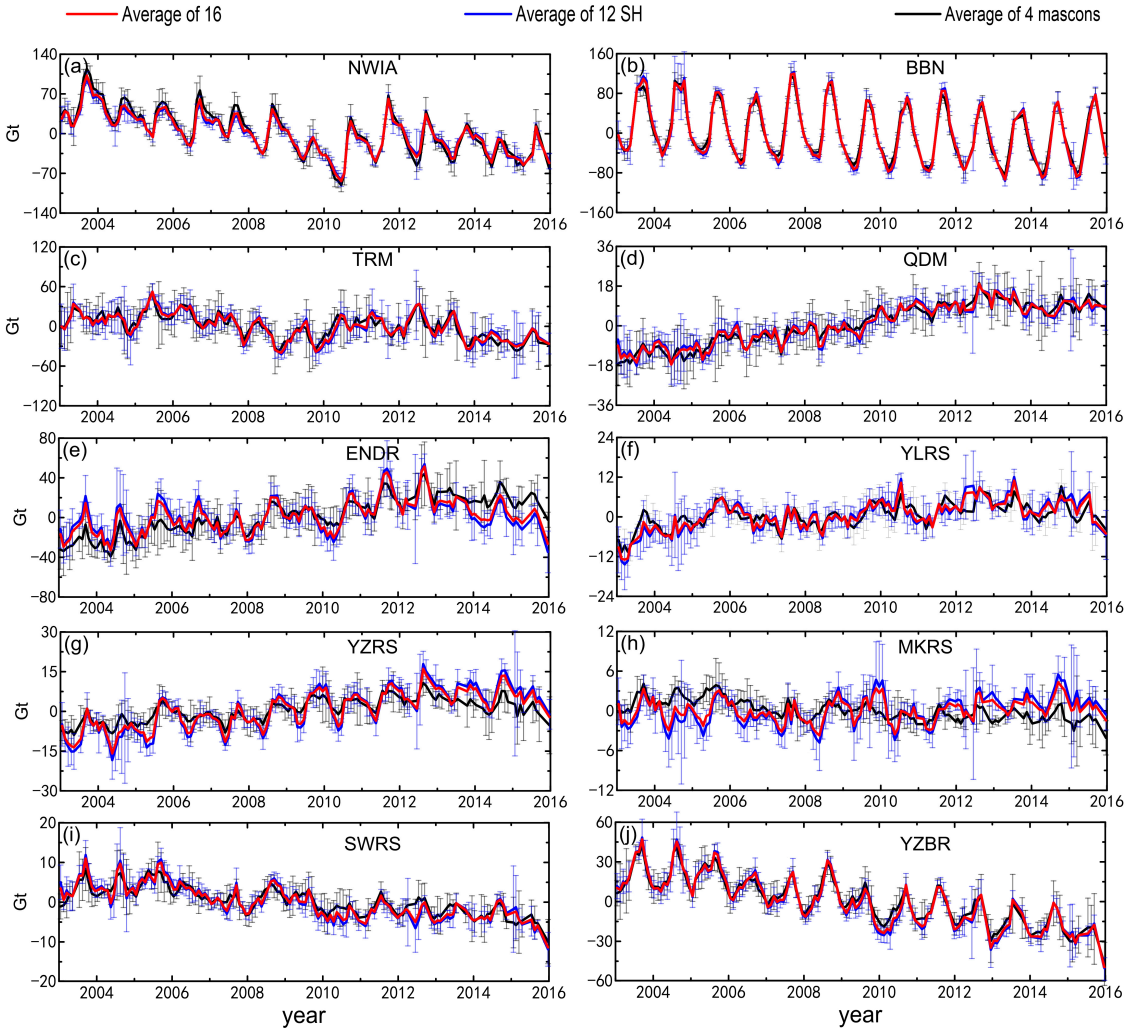

Figure A3. Similar to Figure A1, but showing results for 10 selected water basins: (**a**) NWIA, Northwest India; (**b**) BBN, Bengal Basin; (**c**) TRM, Tarim Basin; (**d**) QDM, Qaidam Basin; (**e**) ENDR, Endorheic Region of the TP; (**f**) YLRS, Yellow River source region; (**g**) YZRS, Yangtze River source Region; (**h**) MKRS, Mekong River source region; (**i**) SWRS, Salween River source region; (**j**) YZBR Yarlung Zangbo River Basin.

Table A1. Pearson's correlation coefficients (PCCs) among the TWS change trends from the inverted solutions shown in Figure 3 and the average of all 16 solutions, marked as 'AVE'. The PCCs are calculated for the whole study area (upper triangular) and for only inside the TP (lower triangular area).

PCC	COST-G	ITSG	GFZ	CSR	JPL	Tongji	HUST	WHU	IGG	AIUB	GRGS	XISM	CSR_M	JPL_M	GSFC_M	ANU_M	AVE
COST-G	1.0000	0.9961	0.9930	0.9919	0.9797	0.9840	0.9925	0.9747	0.9758	0.9925	0.9942	0.9566	0.8016	0.6372	0.7636	0.7695	0.9857
ITSG	0.9940	1.0000	0.9923	0.9892	0.9817	0.9854	0.9898	0.9752	0.9777	0.9925	0.9946	0.9546	0.7985	0.6346	0.7595	0.7696	0.9849
GFZ	0.9871	0.9876	1.0000	0.9863	0.9775	0.9814	0.9888	0.9696	0.9737	0.9884	0.9887	0.9494	0.7962	0.6326	0.7593	0.7607	0.9814
CSR	0.9845	0.9801	0.9718	1.0000	0.9745	0.9759	0.9894	0.9673	0.9739	0.9839	0.9870	0.9576	0.7923	0.6293	0.7476	0.7629	0.9796
JPL	0.9577	0.9616	0.9632	0.9504	1.0000	0.9675	0.9758	0.9571	0.9693	0.9758	0.9802	0.9516	0.7820	0.6184	0.7417	0.7597	0.9719
Tongji	0.9801	0.9740	0.9748	0.9566	0.9212	1.0000	0.9780	0.9882	0.9717	0.9774	0.9818	0.9560	0.8143	0.6502	0.7908	0.7632	0.9827
HUST	0.9859	0.9868	0.9800	0.9823	0.9570	0.9671	1.0000	0.9678	0.9748	0.9849	0.9899	0.9557	0.7947	0.6273	0.7531	0.7600	0.9804
WHU	0.9697	0.9561	0.9528	0.9459	0.9016	0.9830	0.9526	1.0000	0.9639	0.9650	0.9703	0.9468	0.8166	0.6535	0.7996	0.7550	0.9761
IGG	0.9710	0.9761	0.9800	0.9627	0.9647	0.9465	0.9672	0.9102	1.0000	0.9699	0.9758	0.9683	0.7875	0.6389	0.7567	0.7415	0.9736
AIUB	0.9908	0.9910	0.9853	0.9710	0.9583	0.9719	0.9796	0.9630	0.9718	1.0000	0.9896	0.9457	0.7879	0.6282	0.7513	0.7597	0.9785
GRGS	0.9921	0.9936	0.9859	0.9807	0.9680	0.9665	0.9838	0.9502	0.9763	0.9881	1.0000	0.9560	0.7972	0.6341	0.7567	0.7714	0.9835
XISM	0.9506	0.9532	0.9655	0.9392	0.9472	0.9284	0.9507	0.8850	0.9809	0.9494	0.9565	1.0000	0.8018	0.6520	0.7565	0.7504	0.9631
CSR_M	0.5298	0.5002	0.5173	0.4845	0.4218	0.6052	0.4831	0.6063	0.4560	0.5146	0.4859	0.4413	1.0000	0.8295	0.9137	0.8532	0.8760
JPL_M	0.3569	0.3247	0.3483	0.3052	0.2540	0.4325	0.2949	0.4377	0.3037	0.3471	0.3139	0.3011	0.7739	1.0000	0.7723	0.6898	0.7301
GSFC_M	0.6095	0.5792	0.5978	0.5500	0.4872	0.6895	0.5555	0.6907	0.5187	0.5911	0.5662	0.5059	0.9164	0.7574	1.0000	0.7978	0.8384
ANU_M	0.6064	0.6056	0.5862	0.5848	0.5289	0.6115	0.5659	0.6046	0.5609	0.6089	0.5898	0.5352	0.7273	0.5180	0.6966	1.0000	0.8307
AVE	0.9807	0.9739	0.9750	0.9586	0.9308	0.9825	0.9615	0.9681	0.9518	0.9750	0.9693	0.9335	0.6641	0.4948	0.7252	0.7038	1.0000

Table A2. Pearson's correlation coefficients (PCCs) between the average of all 16 GRACE solutions (PCC1) and 12 SH solutions (for SH solutions) or four mascon solutions (for mascons) (PCC2) and TWS change time series at 14 glacier mascons derived from each of the 16 different GRACE SH solutions.

No.	Mascon	COST-G		ITSG		GFZ		CSR		JPL		Tongji		HUST		WHU	
		PCC1	PCC2	PCC1	PCC2	PCC1	PCC2	PCC1	PCC2	PCC1	PCC2	PCC1	PCC2	PCC1	PCC2	PCC1	PCC2
1	Nyainqentanglha	0.99	0.99	0.99	0.99	0.98	0.99	0.97	0.98	0.95	0.95	0.96	0.96	0.97	0.98	0.97	0.95
2	E. Himalayas	0.96	0.96	0.96	0.96	0.97	0.97	0.89	0.89	0.85	0.86	0.95	0.95	0.93	0.93	0.94	0.94
3		0.98	0.99	0.98	0.98	0.98	0.98	0.96	0.96	0.89	0.90	0.97	0.97	0.94	0.94	0.96	0.96
4	W. Himalayas	0.97	0.98	0.98	0.98	0.93	0.94	0.87	0.89	0.90	0.92	0.95	0.94	0.94	0.94	0.97	0.95
5		0.96	0.97	0.97	0.97	0.93	0.93	0.91	0.93	0.47	0.49	0.92	0.89	0.88	0.91	0.89	0.88
6	Karakoram	0.99	0.99	0.98	0.99	0.97	0.98	0.96	0.97	0.80	0.81	0.94	0.93	0.93	0.93	0.95	0.94
7	Hindukush	0.97	0.96	0.98	0.98	0.96	0.96	0.95	0.95	0.85	0.85	0.96	0.96	0.95	0.95	0.94	0.93
8	Pamir	0.98	0.99	0.96	0.97	0.88	0.88	0.91	0.91	0.91	0.92	0.97	0.96	0.93	0.94	0.98	0.96
9		0.99	0.99	0.99	0.98	0.91	0.91	0.96	0.96	0.91	0.91	0.97	0.97	0.94	0.95	0.97	0.97
10	Tien Shan	0.98	0.98	0.98	0.98	0.89	0.90	0.94	0.95	0.94	0.94	0.94	0.94	0.94	0.94	0.97	0.96
11		0.99	0.99	0.99	0.99	0.97	0.97	0.96	0.96	0.97	0.97	0.97	0.97	0.97	0.97	0.98	0.98
12		0.98	0.99	0.98	0.98	0.88	0.89	0.93	0.94	0.90	0.90	0.96	0.96	0.92	0.93	0.97	0.96
13	West Kunlun	0.96	0.96	0.94	0.93	0.86	0.86	0.87	0.87	0.71	0.72	0.94	0.94	0.79	0.80	0.91	0.91
14	Qilian	0.90	0.91	0.77	0.78	0.69	0.68	0.74	0.76	0.63	0.65	0.75	0.73	0.52	0.52	0.65	0.60

No.	Mascon	IGG		AIUB		GRGS		XISM		CSR_M		JPL_M		GSFC_M		ANU_M	
		PCC1	PCC2	PCC1	PCC2	PCC1	PCC2	PCC1	PCC2	PCC1	PCC2	PCC1	PCC2	PCC1	PCC2	PCC1	PCC2
1	Nyainqentanglha	0.97	0.97	0.97	0.97	0.98	0.98	0.93	0.94	0.97	0.99	0.91	0.98	0.94	0.98	0.95	0.93
2	E. Himalayas	0.93	0.93	0.93	0.94	0.95	0.96	0.88	0.88	0.95	0.99	0.93	0.96	0.95	0.98	0.87	0.92
3		0.96	0.96	0.95	0.95	0.98	0.98	0.94	0.94	0.97	0.98	0.94	0.96	0.95	0.96	0.88	0.92
4	W. Himalayas	0.93	0.94	0.93	0.93	0.96	0.96	0.89	0.90	0.96	0.98	0.89	0.96	0.95	0.99	0.91	0.95
5		0.88	0.88	0.91	0.93	0.93	0.94	0.84	0.85	0.78	0.98	0.62	0.91	0.79	0.97	0.85	0.92
6	Karakoram	0.95	0.96	0.92	0.92	0.97	0.97	0.93	0.93	0.87	0.98	0.70	0.88	0.93	0.94	0.74	0.94
7	Hindukush	0.94	0.94	0.94	0.95	0.97	0.97	0.88	0.88	0.97	0.99	0.96	0.98	0.97	0.98	0.94	0.96
8	Pamir	0.92	0.93	0.90	0.91	0.91	0.92	0.88	0.90	0.97	0.99	0.97	0.99	0.95	0.98	0.94	0.97
9		0.97	0.97	0.93	0.93	0.97	0.97	0.91	0.91	0.96	0.98	0.89	0.96	0.93	0.94	0.91	0.97
10	Tien Shan	0.93	0.93	0.94	0.94	0.96	0.96	0.87	0.88	0.95	0.99	0.92	0.97	0.91	0.94	0.91	0.95
11		0.96	0.97	0.97	0.97	0.99	0.98	0.95	0.95	0.98	0.99	0.97	0.98	0.97	0.97	0.95	0.97
12		0.93	0.93	0.93	0.94	0.95	0.95	0.90	0.90	0.96	0.98	0.96	0.97	0.93	0.96	0.88	0.95
13	West Kunlun	0.83	0.84	0.85	0.85	0.92	0.92	0.70	0.72	0.91	0.96	0.82	0.93	0.90	0.91	0.33	0.48
14	Qilian	0.66	0.68	0.41	0.43	0.65	0.65	0.68	0.69	0.54	0.75	0.30	0.67	0.23	0.53	0.36	0.46

Table A3. Similar to Table A2, but showing the results for the PCCs calculated after the annual signals and trends are removed.

No.	Mascon	COST-G		ITSG		GFZ		CSR		JPL		Tongji		HUST		WHU	
		PCC1	PCC2	PCC1	PCC2	PCC1	PCC2	PCC1	PCC2	PCC1	PCC2	PCC1	PCC2	PCC1	PCC2	PCC1	PCC2
1	Nyainqentanglha	0.95	0.96	0.95	0.95	0.90	0.91	0.86	0.88	0.72	0.73	0.83	0.83	0.87	0.89	0.82	0.80
2	E. Himalayas	0.83	0.84	0.77	0.77	0.84	0.85	0.43	0.43	0.59	0.61	0.76	0.76	0.68	0.70	0.70	0.67
3		0.89	0.90	0.84	0.84	0.85	0.86	0.79	0.80	0.57	0.60	0.75	0.74	0.75	0.77	0.80	0.77
4	W. Himalayas	0.93	0.94	0.94	0.94	0.84	0.85	0.76	0.79	0.81	0.83	0.85	0.84	0.85	0.84	0.88	0.84
5		0.95	0.95	0.95	0.94	0.88	0.87	0.87	0.88	0.45	0.47	0.86	0.84	0.84	0.85	0.84	0.82
6	Karakoram	0.97	0.97	0.96	0.96	0.93	0.93	0.90	0.91	0.68	0.69	0.83	0.82	0.83	0.83	0.87	0.85
7	Hindukush	0.89	0.88	0.93	0.93	0.84	0.85	0.82	0.82	0.68	0.70	0.86	0.86	0.81	0.82	0.80	0.77
8	Pamir	0.96	0.97	0.93	0.93	0.79	0.80	0.83	0.84	0.84	0.86	0.93	0.92	0.89	0.90	0.94	0.92
9		0.97	0.97	0.94	0.93	0.72	0.73	0.85	0.86	0.70	0.72	0.88	0.87	0.82	0.83	0.87	0.85
10	Tien Shan	0.96	0.96	0.96	0.95	0.83	0.84	0.89	0.89	0.86	0.88	0.88	0.87	0.87	0.88	0.92	0.91
11		0.90	0.90	0.91	0.91	0.84	0.83	0.73	0.75	0.80	0.80	0.77	0.77	0.75	0.76	0.84	0.83
12		0.95	0.97	0.93	0.94	0.75	0.79	0.85	0.87	0.77	0.78	0.90	0.90	0.81	0.83	0.89	0.86
13	West Kunlun	0.91	0.91	0.84	0.84	0.68	0.68	0.73	0.74	0.57	0.59	0.85	0.83	0.67	0.67	0.78	0.76
14	Qilian	0.90	0.90	0.77	0.77	0.67	0.66	0.73	0.74	0.63	0.65	0.74	0.72	0.51	0.51	0.64	0.60

Table A3. *Cont.*

No.	Mascon	IGG		AIUB		GRGS		XISM		CSR_M		JPL_M		GSFC_M		ANU_M	
		PCC1	PCC2	PCC1	PCC2	PCC1	PCC2	PCC1	PCC2	PCC1	PCC2	PCC1	PCC2	PCC1	PCC2	PCC1	PCC2
1	Nyainqentanglha	0.81	0.80	0.87	0.88	0.88	0.88	0.79	0.79	0.85	0.94	0.79	0.94	0.82	0.91	0.63	0.79
2	E. Himalayas	0.67	0.67	0.78	0.79	0.82	0.83	0.60	0.60	0.65	0.89	0.52	0.84	0.68	0.85	0.57	0.71
3		0.70	0.71	0.68	0.68	0.83	0.84	0.71	0.72	0.81	0.88	0.74	0.87	0.81	0.91	0.49	0.70
4	W. Himalayas	0.83	0.84	0.82	0.83	0.87	0.88	0.72	0.74	0.87	0.94	0.75	0.95	0.83	0.94	0.77	0.86
5		0.79	0.78	0.88	0.89	0.89	0.90	0.72	0.72	0.81	0.94	0.83	0.93	0.79	0.91	0.74	0.88
6	Karakoram	0.91	0.91	0.81	0.81	0.92	0.93	0.84	0.85	0.77	0.95	0.64	0.90	0.81	0.89	0.71	0.91
7	Hindukush	0.83	0.85	0.82	0.83	0.90	0.91	0.75	0.76	0.87	0.96	0.90	0.97	0.88	0.94	0.80	0.89
8	Pamir	0.87	0.88	0.82	0.83	0.84	0.84	0.80	0.83	0.92	0.98	0.92	0.99	0.90	0.96	0.85	0.91
9		0.85	0.85	0.84	0.84	0.89	0.89	0.71	0.72	0.88	0.96	0.81	0.93	0.86	0.88	0.76	0.94
10	Tien Shan	0.86	0.87	0.89	0.89	0.91	0.92	0.82	0.83	0.91	0.98	0.88	0.96	0.88	0.92	0.82	0.94
11		0.78	0.79	0.78	0.77	0.84	0.85	0.73	0.73	0.80	0.85	0.67	0.83	0.78	0.81	0.69	0.84
12		0.81	0.81	0.84	0.85	0.86	0.86	0.71	0.70	0.89	0.95	0.90	0.94	0.86	0.91	0.76	0.90
13	West Kunlun	0.71	0.73	0.68	0.68	0.81	0.82	0.60	0.63	0.77	0.91	0.61	0.86	0.75	0.78	0.64	0.83
14	Qilian	0.70	0.71	0.40	0.42	0.68	0.67	0.66	0.67	0.59	0.76	0.50	0.76	0.41	0.58	0.40	0.79

Table A4. Similar to Table A2, but showing the results for PCCs at 10 selected water basins.

Area	COST-G		ITSG		GFZ		CSR		JPL		Tongji		HUST		WHU	
	PCC1	PCC2	PCC1	PCC2	PCC1	PCC2	PCC1	PCC2	PCC1	PCC2	PCC1	PCC2	PCC1	PCC2	PCC1	PCC2
NWIA	1.00	1.00	0.99	0.99	0.99	0.99	0.98	0.98	0.98	0.98	0.99	0.99	0.99	0.99	0.98	0.98
BBN	1.00	1.00	1.00	1.00	1.00	1.00	0.99	0.99	0.97	0.97	1.00	1.00	0.99	1.00	0.99	1.00
TRM	0.97	0.97	0.94	0.95	0.89	0.90	0.91	0.92	0.85	0.85	0.90	0.91	0.93	0.93	0.95	0.95
QDM	0.99	0.99	0.98	0.98	0.97	0.97	0.95	0.95	0.96	0.96	0.94	0.94	0.93	0.94	0.94	0.94
ENDR	0.97	0.98	0.95	0.96	0.95	0.96	0.89	0.91	0.91	0.90	0.88	0.91	0.90	0.94	0.91	0.94
YLRS	0.97	0.98	0.96	0.97	0.90	0.93	0.89	0.89	0.92	0.92	0.91	0.92	0.90	0.91	0.91	0.88
YZRS	0.98	0.98	0.98	0.98	0.98	0.98	0.94	0.93	0.94	0.95	0.94	0.95	0.94	0.94	0.95	0.96
MKRS	0.95	0.97	0.91	0.93	0.89	0.92	0.81	0.83	0.69	0.74	0.82	0.81	0.73	0.76	0.79	0.79
SWRS	0.98	0.99	0.98	0.98	0.96	0.96	0.93	0.95	0.94	0.94	0.92	0.93	0.95	0.96	0.94	0.94
YZBR	0.99	0.99	0.99	0.99	0.99	0.99	0.97	0.98	0.97	0.97	0.98	0.98	0.99	0.99	0.96	0.96
Area	**IGG**		**AIUB**		**GRGS**		**XISM**		**CSR_M**		**JPL_M**		**GSFC_M**		**ANU_M**	
	PCC1	PCC2	PCC1	PCC2	PCC1	PCC2	PCC1	PCC2	PCC1	PCC2	PCC1	PCC2	PCC1	PCC2	PCC1	PCC2
NWIA	0.97	0.97	0.99	0.99	0.99	0.99	0.96	0.96	0.99	0.99	0.98	0.99	0.98	0.98	0.97	0.97
BBN	0.98	0.98	0.99	0.99	1.00	1.00	0.98	0.98	0.99	1.00	0.99	1.00	0.99	1.00	0.99	0.99
TRM	0.88	0.88	0.84	0.85	0.88	0.90	0.81	0.78	0.94	0.94	0.92	0.91	0.84	0.81	0.63	0.79
QDM	0.92	0.92	0.92	0.93	0.94	0.94	0.80	0.82	0.93	0.96	0.89	0.93	0.95	0.97	0.86	0.89
ENDR	0.86	0.90	0.90	0.90	0.88	0.89	0.62	0.61	0.92	0.91	0.86	0.96	0.84	0.97	0.49	0.80
YLRS	0.89	0.89	0.91	0.91	0.91	0.93	0.75	0.78	0.80	0.96	0.88	0.94	0.82	0.93	0.65	0.79
YZRS	0.95	0.95	0.90	0.89	0.96	0.96	0.88	0.88	0.84	0.91	0.84	0.95	0.91	0.90	0.73	0.84
MKRS	0.81	0.82	0.84	0.85	0.86	0.89	0.77	0.79	0.17	0.94	0.06	0.93	0.24	0.91	0.42	0.56
SWRS	0.93	0.92	0.95	0.96	0.96	0.96	0.86	0.87	0.93	0.98	0.87	0.95	0.88	0.94	0.70	0.76
YZBR	0.98	0.98	0.98	0.98	0.98	0.98	0.95	0.95	0.98	0.99	0.96	0.97	0.97	0.98	0.91	0.93

Table A5. Similar to Table A3, but showing the results for PCCs at 10 selected water basins.

Area	COST-G		ITSG		GFZ		CSR		JPL		Tongji		HUST		WHU	
	PCC1	PCC2	PCC1	PCC2	PCC1	PCC2	PCC1	PCC2	PCC1	PCC2	PCC1	PCC2	PCC1	PCC2	PCC1	PCC2
NWIA	0.99	0.99	0.98	0.98	0.99	0.99	0.95	0.96	0.96	0.96	0.98	0.98	0.97	0.97	0.97	0.97
BBN	0.99	0.99	0.97	0.98	0.98	0.98	0.95	0.95	0.76	0.78	0.96	0.96	0.95	0.95	0.96	0.95
TRM	0.96	0.96	0.91	0.92	0.88	0.89	0.87	0.87	0.80	0.81	0.83	0.84	0.88	0.89	0.90	0.90
QDM	0.96	0.97	0.91	0.91	0.87	0.88	0.78	0.81	0.83	0.84	0.82	0.80	0.75	0.78	0.88	0.86
ENDR	0.97	0.97	0.92	0.93	0.92	0.93	0.83	0.84	0.84	0.84	0.87	0.87	0.89	0.90	0.89	0.90
YLRS	0.96	0.97	0.95	0.95	0.87	0.89	0.83	0.84	0.88	0.88	0.89	0.89	0.86	0.87	0.89	0.88
YZRS	0.92	0.92	0.90	0.91	0.90	0.90	0.76	0.75	0.75	0.76	0.81	0.81	0.79	0.80	0.80	0.81
MKRS	0.93	0.94	0.87	0.86	0.83	0.83	0.71	0.71	0.59	0.61	0.76	0.74	0.64	0.67	0.72	0.68
SWRS	0.96	0.97	0.95	0.95	0.89	0.90	0.88	0.90	0.84	0.84	0.85	0.86	0.88	0.89	0.88	0.87
YZBR	0.96	0.97	0.95	0.95	0.94	0.95	0.86	0.87	0.78	0.78	0.92	0.91	0.91	0.93	0.87	0.87
Area	**IGG**		**AIUB**		**GRGS**		**XISM**		**CSR_M**		**JPL_M**		**GSFC_M**		**ANU_M**	
	PCC1	PCC2	PCC1	PCC2	PCC1	PCC2	PCC1	PCC2	PCC1	PCC2	PCC1	PCC2	PCC1	PCC2	PCC1	PCC2
NWIA	0.93	0.93	0.97	0.97	0.97	0.97	0.89	0.90	0.96	0.98	0.94	0.98	0.96	0.97	0.93	0.94
BBN	0.81	0.82	0.93	0.94	0.97	0.96	0.83	0.83	0.94	0.97	0.93	0.97	0.95	0.95	0.87	0.92
TRM	0.81	0.82	0.81	0.83	0.80	0.83	0.68	0.65	0.94	0.92	0.87	0.88	0.81	0.83	0.63	0.82
QDM	0.80	0.81	0.73	0.76	0.78	0.79	0.55	0.57	0.85	0.87	0.83	0.89	0.71	0.76	0.52	0.76
ENDR	0.85	0.85	0.85	0.85	0.87	0.87	0.69	0.68	0.86	0.84	0.84	0.85	0.84	0.87	0.50	0.73
YLRS	0.84	0.84	0.87	0.88	0.91	0.91	0.76	0.76	0.89	0.91	0.87	0.91	0.84	0.88	0.73	0.87
YZRS	0.85	0.86	0.72	0.72	0.86	0.87	0.72	0.73	0.83	0.87	0.82	0.93	0.81	0.78	0.66	0.85
MKRS	0.69	0.71	0.74	0.76	0.79	0.79	0.73	0.75	0.56	0.82	0.40	0.76	0.62	0.88	0.52	0.67
SWRS	0.78	0.77	0.89	0.90	0.91	0.91	0.79	0.79	0.82	0.93	0.74	0.89	0.83	0.89	0.60	0.77
YZBR	0.86	0.86	0.91	0.91	0.91	0.92	0.80	0.80	0.90	0.92	0.83	0.92	0.89	0.91	0.73	0.84

References

1. Song, C.; Huang, B.; Ke, L. Modeling and analysis of lake water storage changes on the Tibetan Plateau using multi-mission satellite data. *Remote Sens. Environ.* **2013**, *135*, 25–35. [CrossRef]
2. Song, C.; Huang, B.; Ke, L.; Richards, K.S. Remote sensing of alpine lake water environment changes on the Tibetan Plateau and surroundings: A review. *ISPRS J. Photogramm. Remote Sens.* **2014**, *92*, 26–37. [CrossRef]
3. Yao, T.; Thompson, L.; Yang, W.; Yu, W.; Gao, Y.; Guo, X.; Yang, X.; Duan, K.; Zhao, H.; Xu, B.; et al. Different glacier status with atmospheric circulations in tibetan plateau and surroundings. *Nat. Clim. Chang.* **2012**, *2*, 663–667. [CrossRef]
4. Sun, J.; Zhou, T.; Liu, M.; Chen, Y.; Shang, H.; Zhu, L.; Shedayi, A.A.; Yu, H.; Cheng, G.; Liu, G.; et al. Linkages of the dynamics of glaciers and lakes with the climate elements over the Tibetan Plateau. *Earth-Sci. Rev.* **2018**, *185*, 308–324. [CrossRef]
5. Zhang, G.; Yao, T.; Xie, H.; Yang, K.; Zhu, L.; Shum, C.K.; Bolch, T.; Yi, S.; Allen, S.; Jiang, L.; et al. Response of Tibetan Plateau lakes to climate change: Trends, patterns, and mechanisms. *Earth-Sci. Rev.* **2020**, *208*, 103269. [CrossRef]
6. Qin, Y.; Wu, T.; Zhao, L.; Wu, X.; Li, R.; Xie, C.; Pang, Q.; Hu, G.; Qiao, Y.; Zhao, G.; et al. Numerical modeling of the active layer thickness and permafrost thermal state across Qinghai-Tibetan Plateau. *J. Geophys. Res. Atmos.* **2017**, *122*, 11604–11620. [CrossRef]
7. Jia, Y.; Lei, H.; Yang, H.; Hu, Q. Terrestrial water storage change retrieved by GRACE and its implication in the Tibetan Plateau: Estimating areal precipitation in Ungauged Region. *Remote Sens.* **2020**, *12*, 3129. [CrossRef]
8. Yi, S.; Sun, W. Evaluation of glacier changes in high-mountain Asia based on 10 year GRACE RL05 models. *J. Geophys. Res. Solid Earth* **2014**, *119*, 2504–2517. [CrossRef]
9. Yang, K.; Ye, B.; Zhou, D.; Wu, B.; Foken, T.; Qin, J.; Zhou, Z. Response of hydrological cycle to recent climate changes in the Tibetan Plateau. *Clim. Chang.* **2011**, *109*, 517–534. [CrossRef]
10. Yang, K.; Wu, H.; Qin, J.; Lin, C.; Tang, W.; Chen, Y. Recent climate changes over the Tibetan Plateau and their impacts on energy and water cycle: A review. *Glob. Planet. Chang.* **2014**, *112*, 79–91. [CrossRef]
11. Zhang, G.; Yao, T.; Shum, C.K.; Yi, S.; Yang, K.; Xie, H.; Feng, W.; Bolch, T.; Wang, L.; Behrangi, A.; et al. Lake volume and groundwater storage variations in Tibetan Plateau's endorheic basin. *Geophys. Res. Lett.* **2017**, *44*, 5550–5560. [CrossRef]
12. Neckel, N.; Kropáček, J.; Bolch, T.; Hochschild, V. Glacier mass changes on the Tibetan Plateau 2003–2009 derived from ICESat laser altimetry measurements. *Environ. Res. Lett.* **2014**, *9*, 014009. [CrossRef]
13. Brun, F.; Berthier, E.; Wagnon, P.; Kääb, A.; Treichler, D. A spatially resolved estimate of High Mountain Asia glacier mass balances from 2000 to 2016. *Nat. Geosci.* **2017**, *10*, 668–673. [CrossRef] [PubMed]
14. Meng, X.; Li, R.; Luan, L.; Lyu, S.; Zhang, T.; Ao, Y.; Han, B.; Zhao, L.; Ma, Y. Detecting hydrological consistency between soil moisture and precipitation and changes of soil moisture in summer over the Tibetan Plateau. *Clim. Dyn.* **2018**, *51*, 4157–4168. [CrossRef]
15. Ullah, W.; Guojie, W.; Gao, Z.; Tawia Hagan, D.F.; Bhatti, A.S.; Zhua, C. Observed linkage between Tibetan Plateau soil moisture and South Asian summer precipitation and the possible mechanism. *J. Clim.* **2021**, *34*, 361–377. [CrossRef]
16. Xiang, L.W.; Wang, H.S.; Steffen, H.; Wu, P.; Jia, L.L.; Jiang, L.M.; Shen, Q. Groundwater storage changes in the Tibetan Plateau and adjacent areas revealed from GRACE satellite gravity data. *Earth Planet. Sci. Lett.* **2016**, *449*, 228–239. [CrossRef]
17. Xiang, L.; Wang, H.; Steffen, H.; Qiao, B.; Feng, W.; Jia, L.; Gao, P. Determination of Weak Terrestrial Water Storage Changes from GRACE in the Interior of the Tibetan Plateau. *Remote Sens.* **2022**, *14*, 544. [CrossRef]
18. Jing, W.; Zhang, P.; Zhao, X. A comparison of different GRACE solutions in terrestrial water storage trend estimation over Tibetan Plateau. *Sci. Rep.* **2019**, *9*, 1765. [CrossRef]
19. Xiang, L.; Wang, H.; Steffen, H.; Jiang, L.; Shen, Q.; Jia, L.; Su, Z.; Wang, W.; Deng, F.; Qiao, B.; et al. Two Decades of Terrestrial Water Storage Changes in the Tibetan Plateau and Its Surroundings Revealed through GRACE/GRACE-FO. *Remote Sens.* **2023**, *15*, 3505. [CrossRef]
20. Peltier, W.R.; Argus, D.F.; Drummond, R. Space geodesy constrains ice-age terminal deglaciation: The global ICE-6G_C (VM5a) model. *J. Geophys. Res. Solid Earth* **2015**, *120*, 450–487. [CrossRef]
21. Landerer, F. Monthly Estimates of Degree-1 (Geocenter) Gravity Coefficients, Generated from GRACE (04-2002-06/2017) and GRACE-FO (06/2018 onward) RL06 Solutions, GRACE Technical Note 13, The GRACE Project, NASA Jet Propulsion Laboratory. 2021. Available online: https://podaac.jpl.nasa.gov/gravity/grace-documentation (accessed on 17 April 2023).
22. Loomis, B.D.; Rachlin, K.E.; Wiese, D.N.; Landerer, F.W.; Luthcke, S.B. Replacing GRACE/GRACE-FO C30 with Satellite Laser Ranging: Impacts on Antarctic Ice Sheet Mass Change. *Geophys. Res. Lett.* **2020**, *47*, e2019GL085488. [CrossRef]
23. Kvas, A.; Behzadpour, S.; Ellmer, M.; Klinger, B.; Strasser, S.; Zehentner, N.; Mayer-Gürr, T. ITSG-Grace2018: Overview and evaluation of a new GRACE-only gravity field time series. *J. Geophys. Res. Solid Earth* **2019**, *124*, 9332–9344. [CrossRef]
24. Bettadpur, S. *UTCSR Level-2 Processing Standards Document for Level-2 Product Release 0005*; GRACE 327-742, CSR-GR-12-xx; Center for Space Research University: Austin, TX, USA, 2012; p. 17.
25. Meyer, U.; Jaeggi, A.; Dahle, C.; Flechtner, F.; Kvas, A.; Behzadpour, S.; Mayer-Gürr, T.; Lemoine, J.M.; Bourgogne, S. *International Combination Service for Time-Variable Gravity Fields (COST-G) Monthly GRACE Series*; GFZ Data Services: Potsdam, Germany, 2020.
26. Dahle, C.; Flechtner, F.; Gruber, C.; König, D.; König, R.; Michalak, G.; Neumeyer, K.H. *GFZ GRACE Level-2 Processing Standards Document for Level-2 Product Release 0005*; Scientific Technical Report-Data; Deutsches GeoForschungsZentrum GFZ: Potsdam, Germany, 2012; Volume 12.
27. Watkins, M.M.; Wiese, D.N.; Yuan, D.N.; Boening, C.; Landerer, F.W. Improved methods for observing Earth'stime variable mass distribution with GRACE using spherical cap mascons. *J. Geophys. Res. Solid Earth* **2015**, *120*, 2648–2671. [CrossRef]

28. Chen, Q.; Shen, Y.; Zhang, X.; Chen, W.; Hsu, H. Tongji-GRACE01: A GRACE-only static gravity field model recovered from GRACE Level-1B data using modified short arc approach. *Adv. Space Res.* **2015**, *56*, 941–951. [CrossRef]
29. Zhong, B.; Li, X.; Chen, J.; Li, Q.; Lu, B. *WHU-GRACE-GPD01s: Monthly Gravity Field Models Derived from GRACE Intersatellite Geopotential Differences*; GFZ Data Services: Potsdam, Germany, 2022. [CrossRef]
30. Zhou, H.; Zhou, Z.; Luo, Z. A New Hybrid Processing Strategy to Improve Temporal Gravity Field Solution. *J. Geophys. Res. Solid Earth* **2019**, *124*, 9415–9432. [CrossRef]
31. Lemoine, J.M.; Biancale, R.; Reinquin, F.; Bourgogne, S.; Gégout, P. *CNES/GRGS RL04 Earth Gravity Field Models, from GRACE and SLR Data*; GFZ Data Services: Potsdam, Germany, 2019.
32. Wang, C.Q.; Xu, H.Z.; Zhong, M.; Feng, W.; Ran, J.J.; Yang, F. An investigation on GRACE temporal gravity field recovery using the dynamic approach. *Chin. J. Geophys.* **2015**, *58*, 756–766.
33. Darbeheshti, N.; Lasser, M.; Meyer, U.; Arnold, D.; Jaeggi, A. *AIUB-G3P GRACE Monthly Gravity Field Solutions*; GFZ Data Services: Potsdam, Germany, 2023. [CrossRef]
34. Xiao, Y.; Xia, Z.; Sun, Z.; Pang, Z. Application of an Improved Dynamic Method Baseline Method to Satellite Gravtimetry Data Processing. *Geomat. Inf. Sci. Wuhan Univ.* **2011**, *36*, 280–284.
35. Save, H.; Bettadpur, S.; Tapley, B.D. High-resolution CSR GRACE RL05 mascons. *J. Geophys. Res. Solid Earth* **2016**, *121*, 7547–7569. [CrossRef]
36. Loomis, B.D.; Luthcke, S.B.; Sabaka, T.J. Regularization and error characterization of GRACE mascons. *J. Geod.* **2019**, *93*, 1381–1398. [CrossRef] [PubMed]
37. Tregoning, P.; McGirr, R.; Pfeffer, J.; Purcell, A.; McQueen, H.; Allgeyer, S.; McClusky, S.C. ANU GRACE data analysis: Characteristics and benefits of using irregularly shaped Mascons. *J. Geophys. Res. Solid Earth* **2022**, *127*, e2021JB022412. [CrossRef]
38. Swenson, S.; Wahr, J. Post-Processing Removal of Correlated Errors in GRACE Data. *Geophys. Res. Lett.* **2006**, *33*, L08402. [CrossRef]
39. Jekeli, C. Alternative methods to smooth the Earth's gravity field. In *Reports of the Department of Geodetic Science and Surveying*; Report No. 327; Ohio State University: Columbus, OH, USA, 1981.
40. Wahr, J.; Molenaar, M.; Bryan, F. Time variability of the Earth's gravity field: Hydrological and oceanic effects and their possible detection using GRACE. *J. Geophys. Res. Solid Earth* **1998**, *103*, 30205–30229. [CrossRef]
41. Wang, H.; Xiang, L.; Jia, L.; Jiang, L.; Wang, Z.; Hu, B.; Gao, P. Load Love numbers and Green's functions for elastic Earth modelsPREM, iasp91, ak135, and modified models with refined crustal structure from Crust 2.0. *Comput. Geosci.* **2012**, *49*, 190–199. [CrossRef]
42. Jacob, T.; Wahr, J.M.; Pfeffer, W.T.; Swenson, S.C. Recent contributions of glaciers and ice caps to sea level rise. *Nature* **2012**, *482*, 514–518. [CrossRef] [PubMed]
43. Li, P.F.; Tong, X.F.; Li, P.J. A Regularized Iterative Algorithm for Solving over-determined Ill-conditioned Linear Equations. *Comput. Digit. Eng.* **2018**, *46*, 1501–1504.
44. Mao, X.J.; Yang, L.Y. A simple iteration algorithm for morbid state linear equation group. *Comput. Tech. Geophys. Geochem. Explor.* **1999**, *21*, 14–18.
45. Farinotti, D.; Longuevergne, L.; Moholdt, G.; Duethmann, D.; Mölg, T.; Bolch, T.; Voro-gushyn, S.; Güntner, A. Substantial glacier mass loss in the Tien Shan over the past 50 years. *Nat. Geosci.* **2015**, *8*, 716–722. [CrossRef]
46. Mu, Y.; Liu, X.; Wang, L. A Pearson's correlation coefficient based decision tree and its parallel implementation. *Inf. Sci.* **2018**, *435*, 40–58. [CrossRef]
47. Despotovic, M.; Nedic, V.; Despotovic, D.; Cvetanovic, S. Evaluation of empirical models for predicting monthly mean horizontal diffuse solar radiation. *Renew. Sustain. Energy Rev.* **2016**, *56*, 246–260. [CrossRef]
48. Li, M.F.; Tang, X.P.; Wu, W.; Liu, H.B. General models for estimating daily global solar radiation for different solar radiation zones in mainland China. *Energy Convers. Manag.* **2013**, *70*, 139–148. [CrossRef]